POLITECNICO DI TORINO
Repository ISTITUZIONALE

Deep Q-networks for an optimal placement of viscous dampers in 2D multi-story linear frames

Original
Deep Q-networks for an optimal placement of viscous dampers in 2D multi-story linear frames / De Iuliis, M., Miceli, E., Castaldo, P.. - In: STRUCTURES. - ISSN 2352-0124. - 94:(2026), pp. 1-20. [10.1016/j.istruc.2026.113329]

Availability:
This version is available at: 11583/3018020 since: 2026-11-17T13:46:42Z

Publisher:
Elsevier

Published
DOI:10.1016/j.istruc.2026.113329

Terms of use:

This article is made available under terms and conditions as specified in the corresponding bibliographic description in the repository

Publisher copyright

(Article begins on next page)

29 November 2026

Structures 94 (2026) 113329

Contents lists available at ScienceDirect

Structures

journal homepage: www.elsevier.com/locate/structures

Deep Q-networks for an optimal placement of viscous dampers in 2D multi-story linear frames

M. De Iuliis *, E. Miceli, P. Castaldo

Department of Structural, Geotechnical and Building Engineering (DISEG), Politecnico di Torino, Turin, Italy

ARTICLE INFO

Keywords:
Optimal placement
Viscous dampers
Deep Q-networks (DQN)
Interstory drift
Structural vibration control
Seismic ground motion

ABSTRACT

This study proposes a reinforcement learning-based framework for the optimal placement of viscous dampers in multi-story frames, with a focus on enhancing structural performance under seismic excitations. A deep Q-Network (DQN) algorithm is developed to identify the most effective damper configurations across the structure, aiming to minimize peak interstory drift. In the literature, different solutions have been proposed mainly focusing on the characteristics of the structural system rather than on the variability of single seismic excitations. The proposed approach is designed to cope with the non-linear and highly variable nature of the cost function, which poses significant challenges to traditional optimization techniques. Therefore, the effectiveness of the DQN approach has been investigated by considering 85 seismic ground motions having various characteristics with the aim of defining the optimal arrangement of the same number of viscous dampers in a ten-story benchmark frame, with respect to the features of each record. To verify the effectiveness of the proposed algorithm, the results were, first, compared with those achievable through a simple uniform distribution strategy for damping, subsequently, tested to ensure their correspondence with the minimum points of the cost function by means of a sensitivity analysis. Finally, the DQN approach was further compared with three optimization methods: gradient descent, genetic algorithm and particle swarm optimization. The results confirm the potential of the reinforcement learning DQN algorithm as an effective optimization tool within performance-based seismic design.

1. Introduction

The issue of seismic control in civil engineering structures, specifically aimed at preventing collapse and safeguarding the lives of occupants, has been one of the most extensively researched topics in recent decades. Nearly 50 years have passed since the pioneering studies of Kelly [1] and Megget [2] on base isolation concepts, as well as the idea of integrating extra-structural damping devices within framed structural systems [3–7]. Passive protection systems, including strategies that involve their combination [8,9], remain among the most widely used in practical applications due to their proven effectiveness and simplicity. As a result, seismic codes in countries with high seismic hazard [10–12] provide guidelines for their use in both new and existing structures as retrofit techniques.

Despite the evolution of these technologies and their general acceptance, several design issues still require further investigation, particularly regarding how to effectively integrate research findings into practical procedures. One of the most significant challenges is the optimal distribution of discrete extra-structural damping devices within framed structures. The seismic response of these systems is strongly influenced by the distribution of the viscous dampers, whose optimal placement primarily depends on the dynamic properties of the incoming seismic signal as well as on the mechanical characteristics of the structural system. A direct approach to this problem is impractical due to the combinatorial explosion phenomenon, which makes it quite impossible to test all configurations, even with a limited number of positions and devices. Consequently, numerical methods have been developed over the years to optimize objective functions related to interstory displacement, internal forces, accelerations, energy indices and structural damage. In his key contributions, Takewaki [13] introduced a method that minimizes the sum of amplitudes of transfer functions related to interstory displacements, evaluated at the natural frequencies of the undamped structure, while considering the total damping provided by the added devices. This method is notable for its ease of application, but it does not account for the incoming seismic excitation. Garcia Lopez [14] further simplified the approach to the problem through a sequential search algorithm that could be easily integrated into conventional design procedures. Aydin et al. [15] employed a similar approach, using

* Corresponding author.
E-mail addresses: massimiliano.deiuliis@polito.it (M. De Iuliis), elena.miceli@polito.it (E. Miceli), paolo.castaldo@polito.it (P. Castaldo).

https://doi.org/10.1016/j.istruc.2026.113329
Received 5 November 2025; Received in revised form 7 April 2026; Accepted 13 October 2026
2352-0124/© 2026 The Authors. Published by Elsevier Ltd on behalf of Institution of Structural Engineers. This is an open access article under the CC BY license (http://creativecommons.org/licenses/by/4.0/).

base shear force as variable, whereas Fujita et al. [16] advanced the optimization method for a fixed number of dampers by using the maximum value of the transfer function amplitudes for interstory drifts along the height of the building as objective function. Lavan and Levy [17] used a different method to address the problem of optimally allocating the minimum dissipative resource required to achieve a specified performance level. They solved an equivalent optimization problem where the added damping was constrained by a maximum weighted integral of the squared angular drift. Lavan and Dargush [18] tackled the same problem using a genetic algorithm to evaluate the Pareto front, considering both the peak interstory displacement and peak absolute acceleration as objectives. For non-linear dampers, Adachi et al. [19] proposed an optimal design scheme aimed at minimizing either the peak relative displacement between floors or the peak acceleration of the top floor through a method based on static condensation and energy equivalence of the dampers. Yahyazadeh and Yakhchalian [20] investigated the impact of different distributions of linear and non-linear viscous dampers on the residual interstory drift ratio using incremental dynamic analysis.

In recent years, various optimization techniques have been developed to address the issue of optimal placement of supplementary damping devices in structural systems. These methods can generally be classified into gradient-based techniques, heuristic approaches and evolutionary strategies. While each of these approaches offers distinct benefits and is suitable for specific types of problems, they also share common drawbacks that must be considered in real-world applications. Gradient-driven approaches, such as those based on gradient descent, are widely used for their simplicity and efficiency in solving optimization problems with smooth cost functions. However, these methods typically assume a fixed structural model and rely on a single seismic ground motion for optimization, which may not capture the variability of real seismic events. This limitation can lead to suboptimal solutions when applied to structures subjected to a wide range of seismic excitations [14,21]. Heuristic techniques, such as those using simulated annealing or particle swarm optimization, and evolutionary algorithms, such as genetic algorithms and differential evolution, offer increased flexibility by seeking solutions in a more non-deterministic manner, enabling a broader exploration of the design space. While these techniques are better suited for managing non-linearities and various design variables, they still face challenges regarding computational efficiency and the ability to generalize across different seismic events [22–26]. Moreover, these methods typically assume that seismic excitation is predictable or remains constant, overlooking the uncertainties in ground motion parameters that can significantly affect the effectiveness of damping devices.

The availability of increasingly powerful and cost-effective computing machines has recently enabled the application of advanced numerical techniques to this problem. These techniques can explicitly account for non-linearities, uncertainties in structural parameters, and generally address more complex models. This topic was also explored by Kangda and Bakre [27], who examined the dynamic behaviour of two buildings connected by linear and non-linear viscous dampers under explosions and seismic excitations. Their findings showed that even though placing every damping device on the top level is not the optimal solution, a significant reduction in structural response is achieved. Sanghai and Pawade [28] developed a method to find the optimal position for friction dampers by considering a model that incorporates non-linear interactions between the structure and the soil. Gomez et al. [29] proposed a methodology where the design of structural elements and extra-structural damping devices is integrated to minimize an objective function using a gradient descent-based method. Recently, Akehashi and Takewaki [30] introduced a method for elastic–plastic planar frame structures subjected to large-amplitude earthquake ground motions, transforming moment frames into shear mass systems to optimize damper placement efficiently. Chan et al. [31] presented Element Exchange and energy-based distribution methods, demonstrating their effectiveness in reducing interstory drift for both two-dimensional ten-story shear buildings and three-dimensional steel moment-resisting frame buildings with variable plan asymmetry. Li et al. [32] developed a dynamic reliability-based optimization framework for simultaneous layout and size design of non-linear viscous dampers, considering uncertainties in seismic excitations and structural parameters. Finally, Hosoda and Fujita [33] studied the robustness of optimal design solutions with respect to uncertainties related to the dynamic characteristics of the devices, while Castaldo and De Iuliis [34] proposed an optimal integrated seismic design procedure aimed at minimizing an objective function related to the design cost. In this context, reinforcement learning (RL) techniques, particularly Deep Q-network (DQN) algorithms, have also been implemented, providing a promising alternative for managing a non-linear, non-convex cost function with a strong dependence on the stochastic nature of ground motions [35,36]. This is due to their ability to handle high-dimensional state-action spaces, model long-term effects through reward shaping, and generalize across diverse seismic inputs, making them well-suited for this class of problems. However, few studies have been conducted so far on the use of this algorithm for seismic-induced vibration control problems. Kim & Kim [37] investigated the effectiveness of the DQN algorithm for a structure with a semi-active mid-story isolation system characterized by magnetorheological devices, comparing the results with well-established algorithms such as Skyhook and Groundhook. In [38], Pisarski & Jankowski examined the effectiveness of the same approach in the case of a span structure equipped with a semi-active device capable of real-time stiffness and damping modification, demonstrating both performance and computational efficiency. Jedlińska et al. [39] studied the case of a structure equipped with a Tuned Mass Damper and a semi-active viscous damper controlled according to the optimal policy evaluated using a DQN algorithm. The results show significantly better performance compared to that of an optimally tuned conventional mass damper. In addition, active systems have recently been investigated. Panda et al. [40] proposed a gradient descent-based RL policy for an active structural control, thoroughly investigated by considering perturbations in model parameters and input forces. The findings from this study indicate that RL-based controllers demonstrate their effectiveness in both continuous and discrete time systems. Gheni et al. [41] presented a deep RL (DRL) framework that modifies linear quadratic regulators to enhance vibration control in building models. The results show that the DRL-based control approach outperforms the classical LQR model in reducing building vibrations. Further recent contributions to the application of deep learning and reinforcement learning in structural vibration control have recently been reported. Cao et al. [42] proposed a physics information enhanced deep neural network (PEDNN) to predict optimal tuning parameters of pendulum-type tandem mass damper-inerter systems for vortex-induced vibration control of super-tall buildings, demonstrating superior accuracy over conventional machine learning approaches. Li et al. [43,44] applied DRL algorithms, including DQN, Deep Deterministic Policy Gradient (DDPG), and Soft Actor-Critic (SAC), to optimize a hybrid base isolation system integrating shape memory alloy-inerter devices, showing that DRL outperforms particle swarm optimization in convergence efficiency. Deep reinforcement learning has also been applied to soil-structure interaction problems, where a DRL-based mesh optimization framework was proposed to achieve an optimal balance between computational accuracy and efficiency in finite element modeling of soil-damped structural systems, enabling local mesh refinement in critical regions while maintaining acceptable accuracy loss under seismic excitations [45].

All these literature studies, together with a comprehensive overview [46] reveal that almost all approaches focus on the structural characteristics of the system without addressing how the variability in the properties of seismic excitations might affect the optimal configuration of the dampers. Furthermore, it highlights that there is a lack of applications of DQN algorithms to the specific problem of optimal placement in elevation of viscous dampers. This study proposes a novel DQN

framework for solving the optimal placement problem, which integrates ground motion variability in the learning phase, to study the effectiveness of this approach for different characteristics of seismic excitations, showing how the variability of the characteristics of the input earthquake leads to very different optimal solutions from each other. In detail, a 2D benchmark regular elastic structural system has been adopted as the ideal case where a uniform distribution of the viscous dampers in different levels allows for suboptimal seismic performance, and 85 seismic ground motions with different characteristics have been considered. For each signal, the optimal placement of the viscous dampers in the ten-story benchmark structure was evaluated. This study aims to demonstrate that seismic excitations with similar characteristics may produce notably different optimal placement solutions, and that the proposed algorithm can efficiently address this variability while maintaining optimal performance. From a practical design perspective, the seismic hazard at a given site is characterized by a limited set of spectrum-compatible accelerograms selected in accordance with seismic design codes. Eurocode 8 [47], for instance, requires a minimum of 3 ground motion records, and recommends at least 7 when the mean structural response is used as the design value, compatible with the site-specific design spectrum for time-history analysis. In this context, the proposed framework would be applied to this limited set of site-specific records, making the computational cost of training a separate agent per record entirely manageable in practice. The use of 85 records in the present study is therefore not a practical requirement but a methodological choice, aimed at investigating the influence of the variability of seismic input characteristics on the optimal damper placement and at demonstrating the generality and robustness of the proposed approach across a wide range of ground motion features. To verify the effectiveness of the proposed algorithm, the obtained results were first compared with those achievable through a simple uniform distribution strategy for damping. Subsequently, a sensitivity analysis was conducted to ensure that the results of the algorithm correspond to the minimum points of the cost function. Finally, to evaluate the effectiveness of the proposed methodology in terms of both computational cost and achieved performance, the obtained results were compared with those of three optimization algorithms widely used in the literature: gradient descent [48], genetic algorithm [49] and particle swarm optimization [50].

This manuscript is organized as follows: Section 2 deals with the dynamic issue, the 2D benchmark elastic structure together with the seismic ground motions considered, highlighting their different characteristics; the DQN optimization algorithm is discussed in Section 3, whereas Section 4 proposes the methodology with applicative choices; Section 5 illustrates the results of the numerical analyses; Section 6 examines the effectiveness of the proposed algorithm in absolute terms and, then, in comparison to the results considering the uniform distribution of viscous dampers. It also evaluates the performance of the DQN approach through a sensitivity analysis. Further, it compares its results with those obtained using gradient descent, genetic algorithm and particle swarm optimization techniques.

2. Optimal viscous damper placement: dynamic issue, case study and seismic ground motions

2.1. Dynamic issue

A shear-type elastic frame, with n degrees of freedom represented by the horizontal relative displacements of each level (Fig. 1), is considered to illustrate the issue. The integration of supplementary viscous damping devices within such a system is aimed at improving seismic performance even in the case of earthquakes with significant intensity.

Viscous dampers are widely used as passive energy dissipation devices in structural engineering, particularly for seismic applications. These devices operate by generating a force that is proportional to the relative velocity between their ends, effectively reducing structural vibrations by converting kinetic energy into heat. They are mathematically described by the linear constitutive law of Eq. (1):

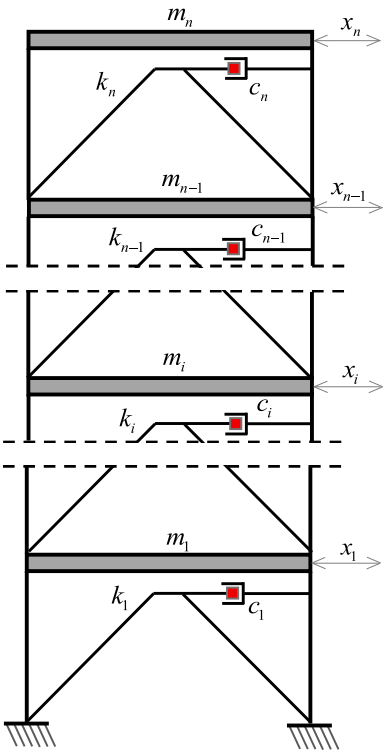

Fig. 1. n degrees of freedom shear-type elastic frame equipped with extra-structural viscous damping.

$$F = c\dot{x} \tag{1}$$

where F is the damping force, c is the damping coefficient of the device and $\dot{x}$ is the relative velocity across the damper. Although nonlinear velocity-dependent dampers are common in practice, linear viscous dampers are routinely used in benchmark studies where the objective is to test a new methodology, rather than to provide a general ready-to-implement device design [51–53]. It is also worth emphasizing that the elastic structural model adopted in this study is consistent with the design philosophy underlying the use of supplemental viscous dampers as prescribed by seismic design codes [47,54]: the number and capacity of the devices can be dimensioned precisely to ensure that the dissipation provided by the complete damper configuration maintains the structural response within the elastic range under the design seismic events. In this context, the elastic assumption represents the target condition of the design process rather than a simplification of the actual structural behavior. Viscous dampers can be arranged in an extra-structural configuration, typically as braces mounted externally to the main structural frame, minimizing disruption to architectural elements and enabling an efficient retrofitting. Their effectiveness in reducing interstory drifts and dissipating seismic energy has been extensively demonstrated through both experimental and analytical studies [55,56].

The behavior of the linear system is described by Eq. (2), expressed in matrix form and accounting for both the inherent damping, modeled using the Rayleigh approach, and the viscous damping provided by supplementary devices potentially placed at each level:

$$\boldsymbol{M}\ddot{\boldsymbol{x}} + (\alpha\boldsymbol{M} + \beta\boldsymbol{K})\dot{\boldsymbol{x}} + \boldsymbol{C}\dot{\boldsymbol{x}} + \boldsymbol{K}\boldsymbol{x} = -\boldsymbol{M}\boldsymbol{I}_g\ddot{u}_g \tag{2}$$

where: **M** is the mass matrix, which defines the mass at each story and influences the inertial response of the structure to seismic excitation, **K** is the stiffness matrix, governing the restoring forces due to structural

deformation, α and β are the Rayleigh damping coefficients used to model the inherent damping of the structure, **C** is the additional viscous damping matrix, representing the energy dissipation introduced by the supplemental damping devices, $\mathbf{I}_g$ is the influence vector, relating ground acceleration to structural response, $\ddot{\mathbf{x}}$, $\dot{\mathbf{x}}$, $\mathbf{x}$ respectively are the vectors of floor accelerations relative to the ground, interstory velocities and interstory drifts.

The design issue of additional damping devices can generally be formulated in two different ways: optimal placement with fixed damping resources (FR) or fixed performance (FP). In the first case, the starting data are the number and capacity of the available devices, which need to be optimally distributed in the different levels to minimize a performance index, P, depending on the system response. In the second case, the objective is to minimize the total capacity of the devices integrated into the structural system to achieve a fixed level of performance of the system, $P = \overline{P}$. In this work, only the FR issue is addressed for two main reasons: first, this case is more commonly applied in practice as a proxy of the construction/retrofit economic cost [15,57], second, an objective of this work is to study the variability of optimal placement as a function of the seismic event characteristics, so that a comparison is useful if the overall viscous damping is constant. It follows that the optimization issue, in the case of elementary viscous damping units, Δc, where the number of units at the i-th floor is d_i, can be formalized as:

"Given n levels, in which m elementary damping units have to be located, the issue is to evaluate within the set $\boldsymbol{D_n}$ of n-tuples $(d_1, d_2, ..., d_n)$ with $d_i \in N$ and $\sum_{i=1}^{n} d_i = m$, the element $(d_1^*, d_2^*, ..., d_n^*)$ such that: $P(d_1^*, d_2^*, ..., d_n^*) = \min[P(d_1, d_2, ..., d_n)]$".

In this formulation, the set $\boldsymbol{D_n}$ represents all possible discrete distributions of the m damping units across the n levels. Each configuration defines a unique allocation scenario and, consequently, leads to a different matrix $\boldsymbol{C}$, which can be written as:

$$\boldsymbol{C} = \begin{bmatrix} (d_1 + d_2)\cdot\Delta c & -d_2\cdot\Delta c & \dots & 0 & 0 \\ -d_2\cdot\Delta c & (d_2 + d_3)\cdot\Delta c & \dots & 0 & 0 \\ \dots & \dots & \dots & \dots & \dots \\ 0 & 0 & \dots & (d_{n-1} + d_n)\cdot\Delta c & -d_n\cdot\Delta c \\ 0 & 0 & \dots & -d_n\cdot\Delta c & d_n\cdot\Delta c \end{bmatrix} \quad (3)$$

Note that the number of elements in the set is equivalent to the number of combinations with replacement of objects into spots, which leads to a complexity having the order of: $O\left(\frac{(n+m-1)!}{m!(n-1)!}\right)$.

2.2. Case study

In the following sections, the design issue will be faced in the case of a benchmark structure represented by a three-bay, ten-story steel frame, which is part of an industrial building constructed in the 1990s [58,59]. This system is schematically represented in Fig. 2 together with a table showing indicative values for the masses and shear stiffnesses corresponding to each level. It is also assumed a Rayleigh damping with a value of 2% for the first two modes, leading to the following values for the Rayleigh coefficients: $\alpha = 0.1785$, $\beta = 0.00185$. Fig. 3 shows the first four modes of the system, normalized with respect to the component at the top level, along with their respective vibration periods. Modal analysis is essential for understanding the dynamic response of structures subjected to seismic loads. In particular, it highlights that, especially in the case of earthquakes with energy concentrated at higher frequencies, capable of exciting higher modes, the structural response is characterized by larger displacements in the upper floors.

For the extra-structural viscous damping to be allocated, a number of $m = 41$ devices will be considered, each elementary unit has the same viscous damping coefficient: $\Delta c = 500000$ Nsec/m. This value is representative of typical damping coefficients used in structural engineering for viscous dampers [60], and it ensures that the system achieves an effective balance between damping and structural flexibility.

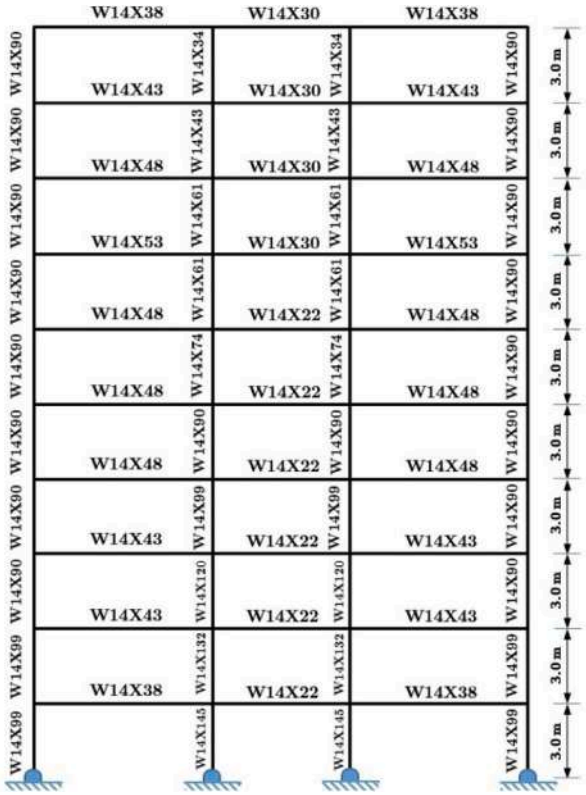

Level	Mass [Kg]	Stiffness [KN/m]
1	50000	108566
2	50000	106592
3	50000	102644
4	50000	96722
5	50000	88826
6	50000	78957
7	50000	67113
8	50000	53296
9	50000	37504
10	50000	19739

Fig. 2. 10-story steel elastic benchmark frame with mass and equivalent lateral stiffness values (modified from [58]).

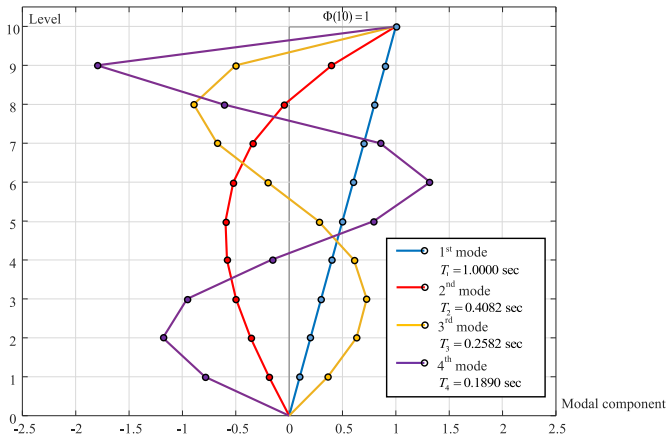

Fig. 3. The first four modes and vibration periods of the benchmark structure.

The selected number of devices corresponds to achieving an overall structural damping equal to 10% of the critical damping when the devices are evenly distributed across the different floors. This damping value is commonly used in seismic applications to achieve a level of damping that significantly reduces resonant vibrations and limits structural damage during strong seismic events.

2.3. Seismic records

A large group of 85 natural seismic events has been selected. These events were chosen for their highly variable characteristics and can be classified into two main sets [61]: 45 far-field (FF) and 40 near-fault (NF) seismic inputs. Each seismic input is identified with a label from 1 to 85, used as reference in the following. Specifically, the FF recordings are divided into 3 subsets based on the PGA/PGV ratio [61] (Fig. 4): high ratio HR (label 1–15), medium ratio MR (label 16–30) and low ratio LR (label 31–45).

On the other hand, the NF recordings (label 46–85) are characterized by higher values of the following indexes:

- Specific Energy Density, SED (Fig. 4), defined as:

$$SED = \int_0^{T_d} \ddot{u}_g^2 dt \tag{4}$$

where T_d is the time duration of the signal above a threshold equal to $0.05g$;

- Power Spectral Density, PSD (Fig. 5), defined as:

$$PSD(f) = \lim_{\Delta t \to \infty} \frac{1}{\Delta t} |X_{\Delta t}(f)|^2 \tag{5}$$

where $X_{\Delta t}(f)$ is the Fourier Transform of the signal (acceleration time history) over a time window of duration Δt, f is the frequency (Hz), $|X_{\Delta t}(f)|^2$ is the squared modulus of the transform (i.e., the power at that frequency). The frequency corresponding to the benchmark structure first mode, $f = 1Hz$, was considered;

- Spectral acceleration, S_a (Fig. 5) corresponding to the peak acceleration experienced by a single-degree-of-freedom (SDOF) system with a given natural period and damping ratio, ξ. The period equal to 1 sec corresponding to the benchmark structure first mode and $\xi = 0.02$ were considered.

These indices used to characterize the seismic excitations have significant physical meanings: the PGA/PGV ratio is a very effective parameter for providing information on the frequency content and duration of ground motions [62,63]; the SED captures the impulsive nature and the energy concentration of seismic events, making it particularly suitable for distinguishing near-fault ground motions. Moreover, SED contains the largest amount of information related to the structural response according to the Shannon entropy metric [64,65]; the PSD describes how the seismic energy is distributed across different frequencies; and the spectral acceleration, S_a, directly correlates ground motion intensity to the expected structural demand at a specific vibration period, providing an essential link between input characteristics and structural performance.

The ground motions considered are all recorded events corresponding to high return periods with highly variable seismic demands and dynamic properties. To represent the different dynamic features of the selected seismic records, Fig. 6 shows the elastic response spectra in terms of peak acceleration (Fig. 6(a)) and displacement (Fig. 6(b)) for 12 significant earthquakes out of the 85 unscaled ones assuming an inherent damping factor of 2%. Fig. 6(a) and Fig. 6(b) clearly show, even though they represent only a significant sample from the group of the 85 records, the great variability of the input signals, both in terms of intensity and frequency content. In detail, the seismic displacement demand at the natural vibration period of the structure (1.0 s) ranges from a few centimetres to over 50 cm for some NF excitations.

In order to characterize the dynamic behavior of the benchmark structure in its original configuration, Fig. 7(a)-(c) show, for the 85 seismic excitations considered: the maximum value of the peak inter-story drifts across levels (i.e., x^{peak}) (Fig. 7(a)), the story in which this

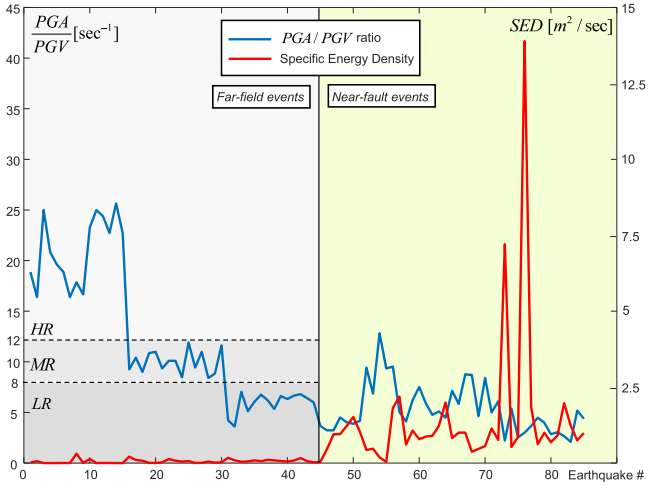

Fig. 4. Classification of the unscaled 85 seismic events.

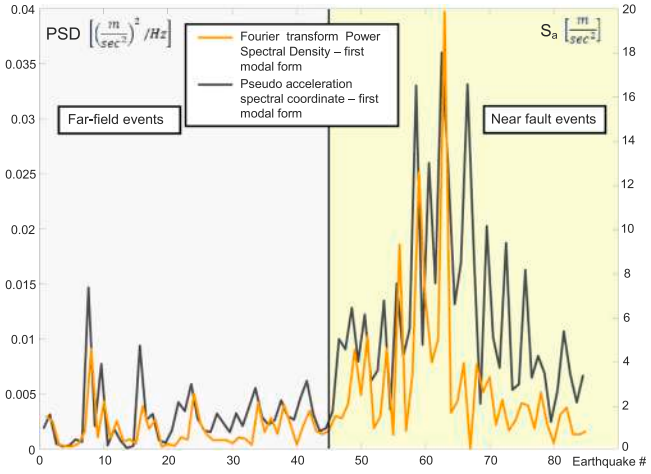

Fig. 5. Classification of the unscaled 85 seismic events.

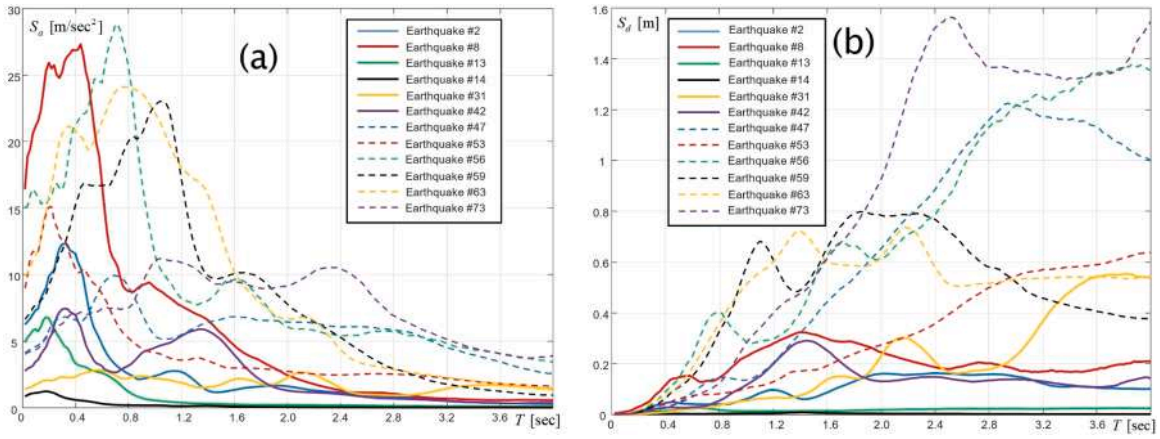

Fig. 6. Response spectra of 12 relevant unscaled seismic ground motions.

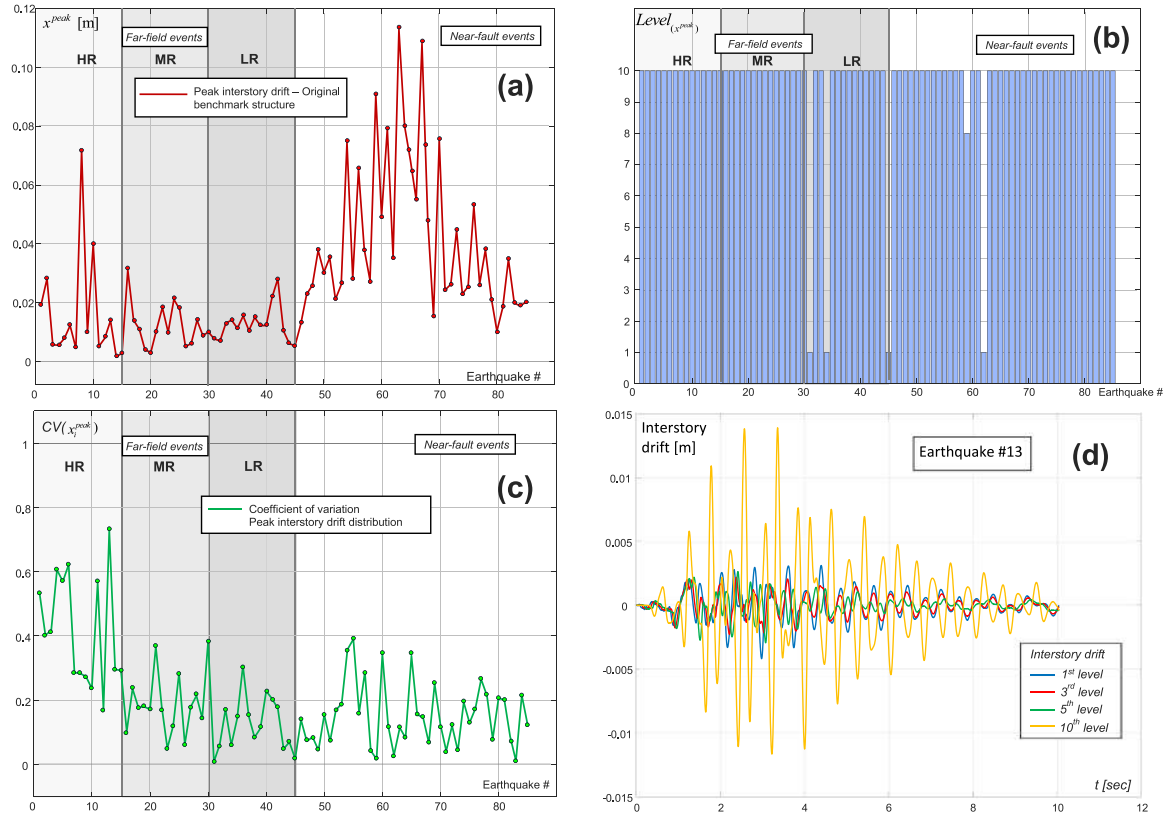

Fig. 7. Dynamic response of the benchmark structure without damping devices.

displacement occurs (Fig. 7(b)), and the coefficient of variation (CV) of the peak interstory displacements corresponding to the different i levels (i.e., x_i^{peak}) (Fig. 7(c)). Finally, in Fig. 7(d), the interstory drift time histories are presented for excitation #13, which exhibits the highest CV. The results show that the maximum value of the peak interstory drifts, typically occurring at 10th level, exceeds 1/150 of the story height for nearly all near-fault excitations and for some far-fault earthquakes, whereas exceeds 1/30 for specific near-fault records. Far-field earthquakes are those that induce a more variable interstory drift demand across different floors, whereas a more uniform response is obtained in the case of near-fault excitations. This highlights the significant seismic vulnerability of the analyzed system, that serves as an ideal subject for examining an optimization process related to a seismic retrofit.

3. Reinforcement learning QND algorithm

Reinforcement learning (RL) is a branch of Machine Learning (ML) which involves the presence of an agent interacting with an environment through well-defined actions and receiving rewards/penalties based on those actions. Through experience and a process of trial and error, the agent gradually learns the optimal decision regarding the future action. RL techniques have demonstrated their effectiveness in recent years, first in the context of games [66], and then in the fields of robotics [67] and finance [68]. RL algorithms, therefore, appear extremely promising in all optimization problems where real-time decisions must be made based on progressively acquired information, making them particularly suitable for use in vibration control [69].

The general RL problem can be formalized as a discrete-time sto-

chastic control process in which an agent interacts with an environment (Fig. 8) obtaining information through observation variables, ψ_τ, and receiving a reward, r_τ, at each step [70]. This process is repeated until the agent reaches a terminal state, t_{end}, when the experience, generally referred to as an "episode", is considered complete and its outcome is defined by the total reward obtained as follows:

$$r_{tot} = \sum_{\tau \le t_{end}} r_\tau \tag{6}$$

The mapping that associates a certain action, or a probability distribution over all possible actions, with each state of the agent is called as "policy", π (either deterministic or probabilistic). An RL algorithm aims to identify an optimal policy, π^*, which maximizes the expected cumulative reward, r_{tot}, in the long term. In this context, the concept of Q-value becomes crucial. The Q-value function assigns to each state-action pair the expected total reward based on the available information, therefore finding the optimal policy means calculating the correct Q-values. RL algorithms are primarily distinguished by the methods used to define the value function: (i) table-based methods or (ii) approaches based on deep learning, such as DQNs. The core idea behind the latter approaches is to use a neural network (NN) to approximate the value function [71].

The DQN algorithm starts by initializing the approximator neural network (Q-network) with randomly set weights. At the same time, a replay buffer is configured, useful to store the agent's experiences at each step in terms of the following data: state, action, reward and next state $(S_{a,\tau}, a_\tau, r_\tau, S_{a,\tau+1})$. This data set is denoted as "transition". During training, at each time step, the agent observes the current state of the environment and selects an action based on the Q-values (i.e., the state-action value function provided by the Q-network). After performing the action, the agent receives a reward and observes the new state of the environment, and the consequential transition is stored in the replay buffer. This process allows the agent to collect data related to the action effects on the environment. Periodically, a batch of transitions is randomly sampled from the replay buffer and used to update the weights of the Q-network. To stabilize the weight updates, a second neural network, called the target network, is used. The target network has the same architecture of the Q-network, but its weights are updated less frequently compared to the Q-network. Specifically, for any transition, the Q-target value is defined using the Bellman expression, as follows:

$$Q_{target}(S_{a,\tau}, a_\tau) = r_\tau + \gamma \cdot \max_{a_{\tau+1}} Q_{target}(S_{a,\tau+1}, a_{\tau+1}) \tag{7}$$

where $0 \le \gamma \le 1$ represents the discount factor, which is a coefficient used to weight future rewards differently from current rewards, and the term $\max_{a_{\tau+1}} Q_{target}(S_{a,\tau+1}, a_{\tau+1})$ is the maximum Q-value estimated by the target network for the new state $S_{a,\tau+1}$ across all possible actions $a_{\tau+1}$. Once the value $Q_{target}(S_{a,\tau}, a_\tau)$ is calculated, the vector representing the weights of the Q-network is updated by minimizing the squared error between the Q-value estimated by the network and the Q-target value:

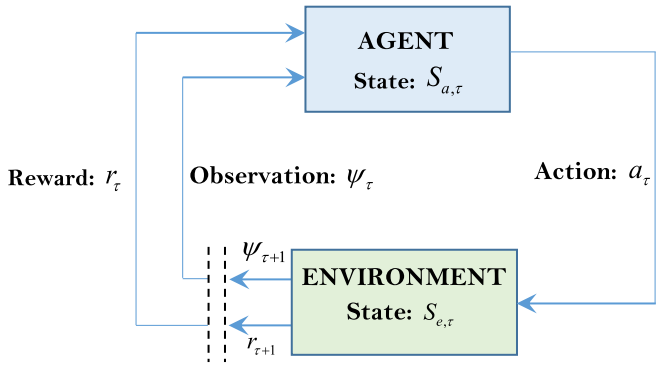

Fig. 8. General framework of RL model.

$$\min_{\omega} \left[Q_{network}(S_{a,\tau}, a_\tau) - Q_{target}(S_{a,\tau}, a_\tau) \right]^2 \tag{8}$$

where $Q_{network}(S_{a,\tau}, a_\tau)$ is the Q-value estimated by the main neural network for the state $S_{a,\tau}$ and action a_τ. The target network remains fixed for a certain number of time steps, thus providing a stable target for updating the Q-network. This methodology allows the DQN algorithm to learn effectively and stably [72], leveraging the neural networks to solve complex and dynamic control problems. A major benefit of DQN in optimizing damper placement, in contrast to other optimization techniques applied in structural challenges (e.g., metaheuristic methods), is its ability to learn from its environment and adapt its strategy over time, potentially offering better scalability in large or dynamic problem areas. While metaheuristics are adept at exploring the search space, DQN employs deep RL to gradually refine its policy, potentially leading to faster convergence and greater efficiency in certain scenarios.

4. Proposal of A DQN algorithm framework for the optimization issue

As described in the previous section, the DQN algorithm can be particularly suitable for active and semi-active control systems. The proposed idea is to adopt the DQN algorithm within the design issue of optimal placement of viscous dampers within a passive control without real-time decisions. In the optimization issue, the agent is represented by the designer who has to place the devices in different levels (i.e., 10 for the benchmark system). In this context, an action is finalised to place a device in a specific position or move an already placed device from a level to another one. The state $S_{a,\tau}$ at step τ is represented as a vector of dimension $n = 10$, where each component d_i denotes the number of elementary damping units currently allocated at the i-th floor:

$$S_{a,\tau} = (d_1,\ d_2,\ d_3,\ d_4,\ d_5,\ d_6,\ d_7,\ d_8,\ d_9,\ d_{10}) \in \mathbb{N}^{10} \text{with} \sum_{i=1}^{10} d_i \le m \tag{9}$$

To ensure numerical compatibility with the Q-network input layer and improve training stability, each component is normalized by the total number of available devices m:

$$\widetilde{d}_i = \frac{d_i}{m}, \widetilde{d}_i \in [0,1] \tag{10}$$

so that the actual input fed into the Q-network is the normalized vector $\widetilde{S}_{a,\tau} = (\widetilde{d}_1, \widetilde{d}_2, \ldots, \widetilde{d}_{10}) \in [0,1]^{10}$. This encoding is compact (dimensionality equal to 10), avoids the sparsity issues associated with one-hot representations, and directly reflects the physical meaning of the allocation state.

The environment, on the other hand, is the benchmark structure subjected to a seismic excitation, and so, the environment is specific for each seismic record. In this way, the agent has a complete observation of the environment and can acquire all the information related to the system's dynamic response. Special attention should be given to definition of the reward: it is assigned once all available devices have been placed since the goal of the design process is to minimize the performance index related to the seismic response of the final design configuration. Therefore, assigning intermediate rewards during the device placement process is avoided, as the agent might maximize the intermediate rewards along the process rather than focusing on achieving the highest possible final reward. This design choice is further motivated by the nature of the problem: since the seismic performance index ρ is only meaningful once all m devices have been placed, as a partially filled configuration does not correspond to a physically admissible damper layout, any intermediate reward based on a partial allocation would be an ill-defined proxy of the actual objective. Even though the reward is zero during the placement phase, the agent is still able to learn an effective placement strategy through the temporal credit assignment mechanism of the DQN: the Q-values of intermediate states are updated

via backpropagation of the Bellman equation (Eq. (7)), so that the expected future reward is propagated back to earlier steps during training. As a result, the agent learns implicitly, over successive episodes, that completing the placement phase leads to states with higher expected reward, which guides the choice between “add” and “move” actions at each intermediate step without requiring any explicit intermediate signal.

This reward structure is moreover fully consistent with the linear elastic assumption adopted for the structural model: the only configuration for which the structural response is evaluated and used to update the agent's policy is the final complete damper layout, which, by design, provides sufficient supplemental dissipation to generally maintain the structural response within the elastic range under the design seismic events.

It follows that this is essentially a path problem on a directed graph with as many layers as the devices to place, with the final layer of order m characterized by a number of nodes equal to $\binom{m+9}{m}$ (Fig. 9). In this directed graph, the node located at position p on the layer ν will be denoted as $\eta_{(\nu;p)}$. Adding a device at a certain level of the structure moves the agent to the next layer, whereas moving a device from a level of the structure to another one corresponds to moving the agent from a node to another one within the same layer. In Fig. 9, the interpretation of the first layer nodes, $\nu = 1$, is straightforward: $\eta_{(1;p)}$ corresponds to the single device placed at the p-th level. The nodes of the first layer, therefore, represent all the possible states of the environment after the first time-step $S_{t=1} = \eta_{(1;p)}$. Only the final layer, where all devices have been allocated, corresponds to a reward that measures the seismic performance of the defined structural configuration.

In the application of the DQN algorithm, some methodological choices and parameter settings are necessary. Firstly, the initial configuration of the state must be determined. The two extreme choices are: (i) the initial state of the environment is the structure without any devices; (ii) all devices are placed according to a fixed rule (e.g., uniform distribution, distribution proportional to the level number). In the first case, the agent's action will be finalised to place sequentially the devices, moving through the graph from the starting point to the last layer (Fig. 9). In the second case, the action will be finalised to swap devices between levels, moving between nodes of the last layer (Fig. 9). In this work, the philosophy, consistent with the objectives, is to guarantee the agent as much freedom as possible. Therefore, it was decided to choose the initial condition where the structure is in the configuration without devices and, as the first step, the only possible action is to add a device. From the second step onwards, the agent can choose between moving a device or adding another one. In particular, the action space $\mathscr{A}$ is discrete and comprises two types of actions: “add” actions a_j^{add}, which place one device on floor $j \in \{1, \ldots, n\}$, available only during the placement phase when $\sum_{i=1}^{n} d_i < m$; “move” actions $a_{j\to k}^{move}$, which transfer one device from floor j to floor k, with $j, k \in \{1, \ldots, n\}$ and $j \neq k$, available only when $d_j > 0$. The total action space size is therefore $n + n(n-1) = n^2 = 100$ for $n = 10$. Illegal actions are prevented through action masking: at each step, the Q-values of unavailable actions are set to $-\infty$ before the ε-greedy selection, so that illegal actions cannot be chosen either during exploration or exploitation.

The logic is that, by not receiving any reward before placing all the devices, the agent learns during the training phase the need to place all the devices and, successively, swap them.

Once all devices are placed, the agent’s task would theoretically be complete. However, exploring alternative placements within the final layer may reveal configurations with improved seismic performance. Therefore, the agent is permitted to perform limited swaps. In the present work, swaps are limited to 50 steps. To justify this choice, a quantitative sensitivity analysis was conducted by evaluating the performance index ρ (Eq. 11) as a function of the number of swaps allowed,

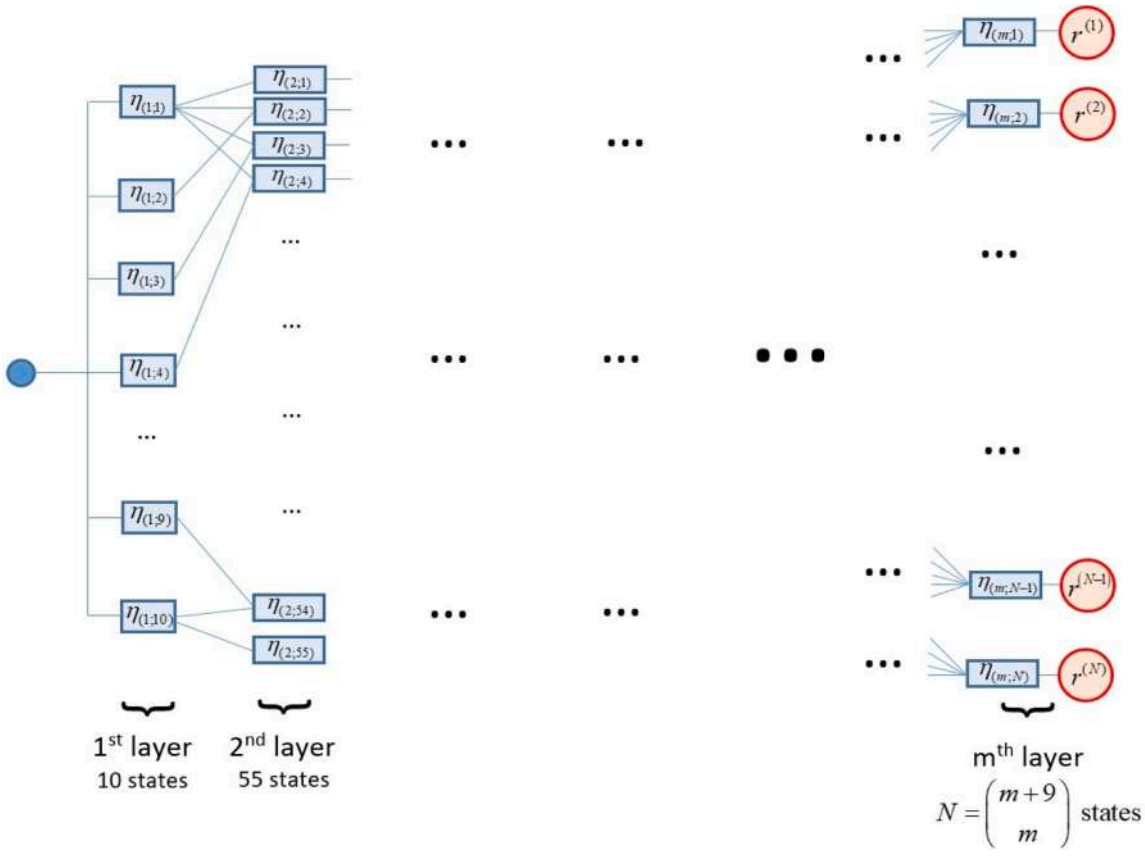

Fig. 9. Directed graph representing the optimal placement issue.

for all 85 seismic records considered. The results are shown in Fig. 10, where the mean value of ρ, normalized with respect to its minimal value (i.e., $\rho_{\min}$), is reported separately for far-field (FF) and near-fault (NF) records for the episode corresponding to the higher performance. The results show that the performance index reaches a plateau well before the 50th swap in all cases, confirming the principle of diminishing returns in local search [67]. Furthermore, the analysis revealed that, in every environment tested, the swap sequence consistently enters a two-cycle oscillatory pattern, where the agent alternates between transferring a device from floor j to floor k and immediately reversing the move, before the 50th swap. The onset of this oscillatory behaviour constitutes a natural convergence criterion for the local search phase, indicating that no further improvement is achievable through additional swaps. The 50-step limit therefore represents a conservative upper bound guaranteeing that convergence has been reached in all cases considered.

A single algorithm episode is thus composed of $w+50$ steps, where $w \geq m$ is the number of steps taken to reach the configuration in which all devices have been placed. This approach aligns with combinatorial optimization strategies, such as Simulated Annealing and Tabu Search, which balance effectiveness with computational efficiency by focusing on a solution's immediate neighbourhood [73–75]. To enhance the clarity of the proposed DQN approach, a schematic flowchart summarizing the key steps of the algorithm as applied to the damper placement issue is provided in Fig. 11.

Another important aspect is how to define the reward once the agent has reached the last layer. In this work, the parameter representing the seismic response is chosen to be equal to the maximum value of the peak interstory drifts (performance index) in the benchmark structure, as follows:

$$\rho = x^{peak} = \max(x_i^{peak}) \quad i = 1, 2, 3..., 10 \tag{11}$$

Although interstory drift is not a complete indicator of the overall damage state of the system, it is the most widely adopted engineering demand parameter (EDP) in performance-based seismic design [34]. Indeed, interstory drift is an appropriate optimization objective [76,77], as a first approach for testing optimization strategies, for several reasons: first, it serves as a direct measure of deformation demand, which can be compared against code-specified drift limits associated with different limit states (e.g., immediate occupancy, life safety, collapse prevention) [78]; second, minimizing drift in the elastic range inherently maintains the structure further from damage thresholds, thereby reducing the likelihood exceeding structural capacity under seismic loading. This approach aligns with common practices in the literature [79–82], where interstory drift is commonly used to evaluate the seismic performance of structures.

The objective of the algorithm is to minimize this quantity, while the agent acts to maximize the rewards. Therefore, the rewards should be defined as a decreasing function $r = f(\rho)$, so that, as ρ decreases, the reward increases. The following choice is both simple and efficient: $r_\tau = -\rho_\tau$. Furthermore, the idea is that at the end of the episode, the sum of the rewards obtained by the agent is indicative of the performance in the last state reached. In this way, with respect to the τ-th step of the episode, the reward will be defined as follows:

$$r_\tau = \begin{cases} 0 & \text{if} \tau < w \\ -\rho_\tau & \text{if} \tau = w \\ -\rho_\tau + \rho_{\tau-1} & \text{if} w < \tau \leq w + 50 \end{cases} \tag{12}$$

which leads, for $\tau > w$, to a positive reward if a reduction in the performance index occurs, whereas the reward will be negative if the maximum value of the peak interstory drifts increases.

The design issue is thus fully described and some hyperparameters typical of the numerical procedure need to be defined to apply the DQN algorithm. In this study, the following values have been set: discount factor $\gamma = 0.99$, replay buffer length equal to 10000, batch size equal to 128, probability of exploring (choosing a random action), instead of exploiting (choosing the action with the highest Q-value) $\varepsilon = 0.3$, which decreases at a rate of 0.01 [83]. An initial sensitivity analysis was carried out to select the values of these hyperparameters. The exploration decay rate (i.e., 0.01) was calibrated to ensure sufficient early-stage exploration without compromising convergence. The replay buffer size (i.e., 10000) and batch size (i.e., 128) were selected to strike a balance between memory diversity and training stability. Finally, the number of episodes was set equal to 500, as performance improvements were observed to plateau beyond this point, while computational costs increased significantly [70]. These choices lead to an exploration-restricted policy for the agent, which is compensated by enough episodes to stabilize the performance. The tuning of hyperparameters allows the DQN algorithm to be highly flexible, enabling it to tackle also more complex problems. Using dimensionality reduction techniques, the framework can effectively handle systems with a larger number of degrees of freedom, such as larger or irregular structures. Additionally, with appropriate adjustments to the state, action and reward definitions, the algorithm can be applied to systems exhibiting non-linear behaviors, both in structural response and in damper behaviour. These non-linearities remain transparent to the DQN algorithm, which interacts with the structural model exclusively through the scalar reward signal, as long as the action space remains discrete, i.e. the optimization concerns the placement of devices of fixed capacity. The extension to a continuous action space, where both placement and device characterization are optimized simultaneously, would instead require alternative deep RL architectures specifically designed for continuous action spaces, such as Deep Deterministic Policy Gradient (DDPG) [84] or Soft Actor-Critic (SAC) [85].

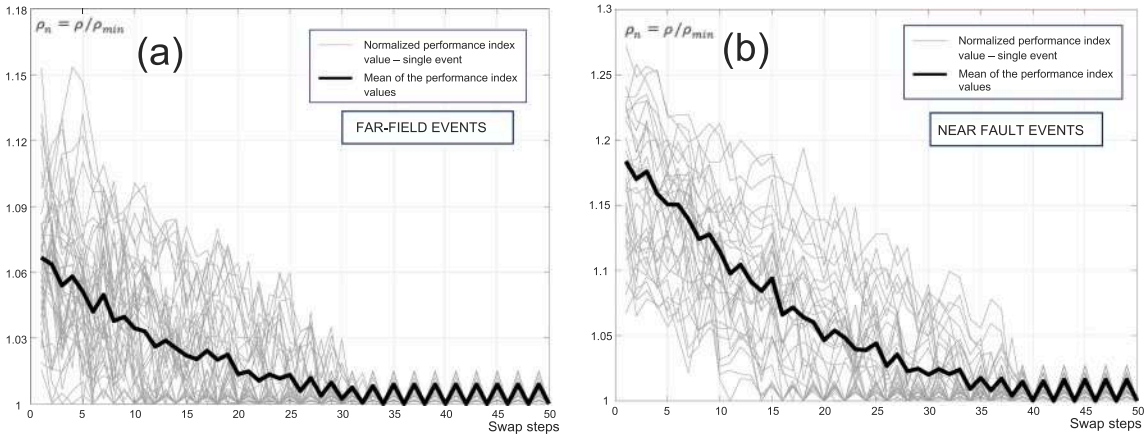

Fig. 10. Sensitivity analysis of the performance index with respect to the number of swap steps - Far Field (a) and Near Fault (b) events.

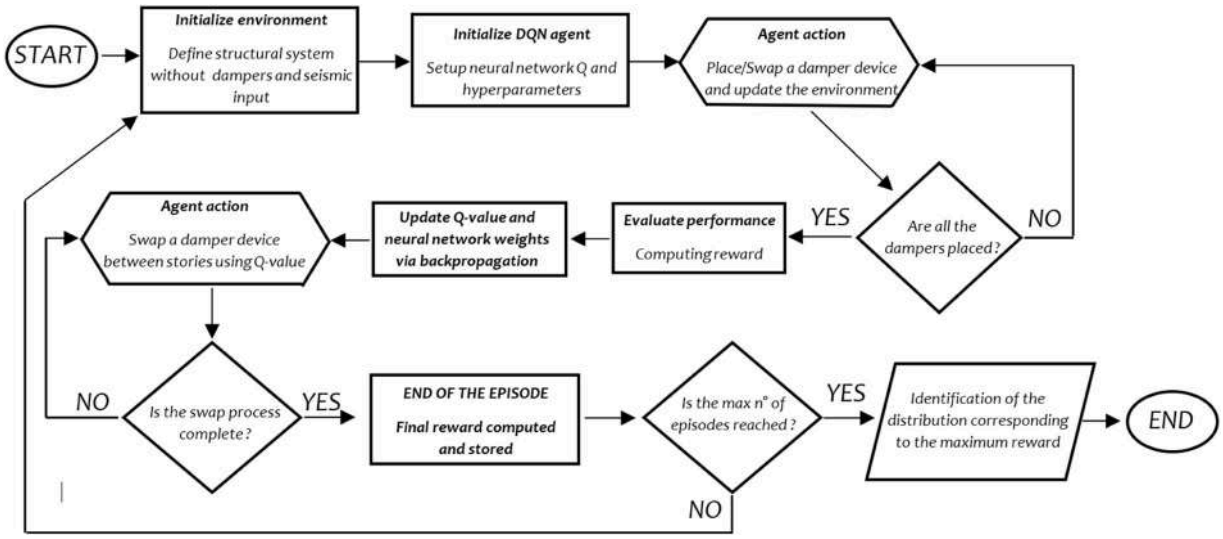

Fig. 11. Flowchart of the DQN algorithm applied to the optimal damper placement problem.

This flexibility makes the DQN approach effective in a wide range of structural configurations and dynamic environments.

5. Optimal placement: results

The DQN RL algorithm, as described in the previous section, has been implemented using the Matlab Reinforcement Learning Toolbox [86] and applied to the issue of optimal placement of viscous dampers for the 85 distinct cases where the structural system is subjected to a single seismic excitation. This algorithm gradually refines the solution, improving it episode by episode, until reaching a point where the performance becomes substantially stable.

As evident from Fig. 12 and Fig. 13, showing the final reward for each episode in the case of a far-field and a near-fault event, this improvement process is not monotonic. This means that there are episodes where the exploratory component, especially during the initial phase, leads to non-optimal configurations. When the final condition, at the 500th episode, is met, the episode corresponding to the maximum reward is recorded, and the distribution of the devices in that episode is taken as the optimal solution. The robustness of the reported solutions with respect to random initialization was verified by repeating the training with different random seeds for a representative subset of records, confirming consistent convergence to equivalent optimal configurations. In Table 1-Table 2, the distribution of the extra-structural viscous dampers across the 10 levels is reported for all cases. There are also reported the maximum value of peak interstory displacements related to the optimal distribution and the Gini index, G, of the distribution [87], which provides a normalized measure of the concentration of the devices across the 10 levels (i.e., $G = 1$ if all the devices are concentrated in a single level, and $G = 0$ if the devices are evenly distributed across the levels).

The main results obtained from the numerical analyses are summarized Fig. 14-Fig. 18. In detail, in Fig. 14(a)-(d), the number of devices placed at the first, third, fifth and tenth levels in the case of optimal arrangement is indicated for each one of the 85 ground motions. These figures show that a greater number of devices is generally placed on the lower floors (i.e., the first or second level) and this number tends to decrease progressively towards the upper floors. The exception is the third level, represented in Fig. 14(b).

Fig. 15 shows the value of the Gini index as a function of the

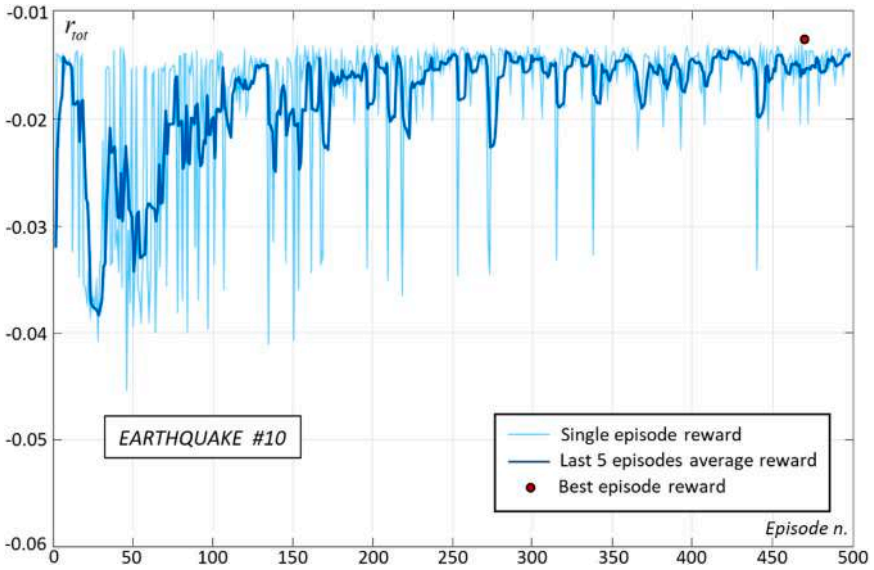

Fig. 12. Progression of the DQN algorithm in searching for the optimal solution (for a far-field event).

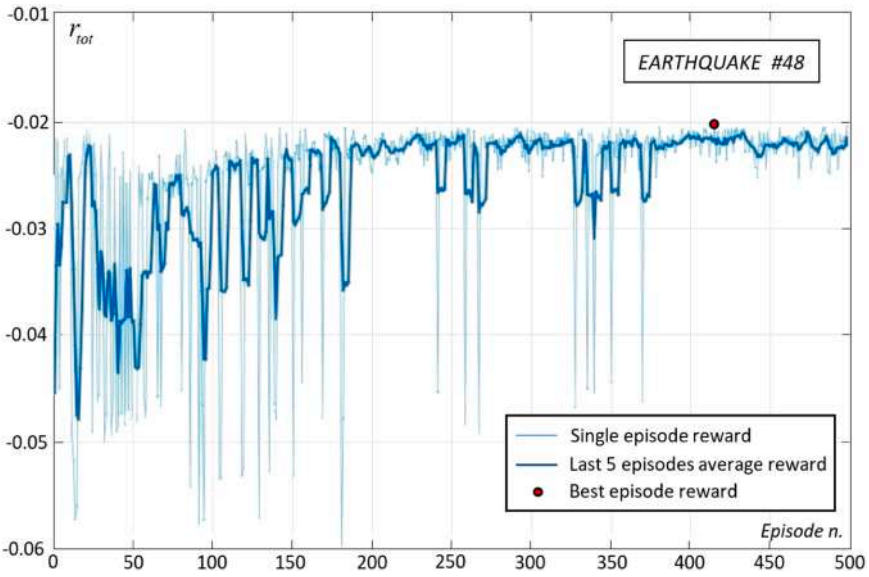

Fig. 13. Progression of the DQN algorithm in searching for the optimal solution (for a near-fault event).

Table 1
Optimal DQN extra-structural damping distribution for far-field events. Units of measure is [Nsec/m].

Earthq. #	*Level 1*	*Level 2*	*Level 3*	*Level 4*	*Level 5*	*Level 6*	*Level 7*	*Level 8*	*Level 9*	*Level 10*	*Gini index*	*Peak interstory drift [m]*
1	6000000	0	0	1000000	0	5500000	4000000	0	2500000	1500000	0.6531	0.00314
2	0	4500000	2500000	0	3500000	0	3500000	3000000	2000000	1500000	0.4743	0.00544
3	5000000	1500000	0	3500000	0	5000000	0	2000000	2000000	1500000	0.5393	0.00121
4	5500000	0	0	0	3000000	5500000	0	2000000	3000000	1500000	0.6098	0.00085
5	500000	4000000	0	2500000	3000000	0	0	5000000	3500000	2000000	0.5339	0.00125
6	4000000	2500000	0	1000000	2000000	4500000	0	1500000	3000000	2000000	0.4417	0.00212
7	5500000	500000	0	2000000	0	3000000	2000000	4500000	3000000	0	0.5610	0.00129
8	500000	4000000	0	3500000	0	3500000	5000000	1500000	1000000	1500000	0.5176	0.02219
9	3500000	2500000	0	0	4500000	4500000	0	1500000	2500000	1500000	0.5068	0.00367
10	2000000	5000000	500000	500000	1000000	5500000	0	2000000	2500000	1500000	0.5122	0.01404
11	1000000	1000000	2000000	6000000	2000000	0	1000000	3000000	3000000	1500000	0.4417	0.00109
12	3500000	4500000	0	2000000	0	0	3000000	3000000	3000000	1500000	0.4634	0.00261
13	4000000	500000	0	4000000	2500000	500000	2500000	2500000	2500000	1500000	0.3984	0.00177
14	5500000	0	0	1500000	2500000	1500000	2000000	3500000	2500000	1500000	0.4472	0.00038
15	0	4500000	1000000	4000000	2000000	500000	0	4000000	3000000	1500000	0.5014	0.00086
16	5500000	4000000	0	0	3000000	0	3000000	2500000	1500000	1000000	0.5393	0.01334
17	6000000	3000000	0	0	0	1000000	3500000	2500000	3000000	1500000	0.5440	0.00503
18	5500000	0	500000	1500000	500000	5000000	1500000	4000000	500000	1500000	0.5501	0.00494
19	6000000	3000000	0	3000000	2500000	1000000	3500000	1000000	500000	0	0.5339	0.00159
20	4000000	3500000	500000	3000000	3000000	3000000	0	2000000	1000000	500000	0.4146	0.00108
21	3500000	2500000	0	0	5000000	3000000	2000000	500000	2500000	1500000	0.4634	0.00299
22	5000000	3500000	0	2500000	2000000	1000000	2500000	2000000	2000000	0	0.4255	0.00700
23	0	9000000	0	2000000	0	3000000	0	2000000	3000000	1500000	0.6694	0.00557
24	5000000	1000000	0	500000	0	3500000	3000000	3500000	2500000	1500000	0.4959	0.00800
25	5500000	0	0	0	3000000	4000000	0	4000000	2500000	1500000	0.5827	0.00381
26	4000000	4500000	0	2500000	500000	0	2500000	2500000	2500000	1500000	0.4417	0.00296
27	6000000	4000000	0	0	4000000	4000000	0	1000000	0	1500000	0.6206	0.00292
28	10500000	0	0	0	0	3000000	0	4000000	3000000	0	0.7940	0.00464
29	1000000	4000000	0	500000	1500000	2500000	3500000	3500000	2500000	1500000	0.3984	0.00374
30	0	5500000	0	0	1000000	3000000	3000000	4000000	2500000	1500000	0.5393	0.00222
31	6000000	4000000	0	0	3500000	0	3000000	2500000	0	1500000	0.5935	0.00619
32	4000000	4500000	0	0	2000000	3000000	3000000	0	2500000	1500000	0.4797	0.00309
33	2000000	0	0	2000000	5500000	5500000	3000000	2000000	500000	0	0.5827	0.00631
34	7000000	0	0	0	4500000	3500000	3000000	0	2500000	0	0.6694	0.00738
35	6500000	0	0	0	5000000	0	2500000	2500000	2500000	1500000	0.6206	0.00496
36	0	4000000	0	2000000	0	2000000	3000000	4500000	3500000	1500000	0.4905	0.00363
37	6000000	0	0	0	3500000	0	4500000	2500000	2500000	1500000	0.6043	0.00409
38	5500000	0	0	4000000	3500000	3000000	2500000	0	500000	1500000	0.5610	0.00592
39	5500000	0	0	3500000	3500000	2500000	3000000	1500000	0	1000000	0.5339	0.00378
40	3500000	3500000	0	4500000	0	0	2500000	2500000	2500000	1500000	0.4634	0.00388
41	0	500000	0	6500000	0	0	5000000	4000000	3000000	1500000	0.6694	0.00768
42	0	7000000	0	4500000	0	5000000	0	1500000	1500000	1000000	0.6802	0.01098
43	5500000	3500000	0	4500000	0	3000000	1000000	1000000	2000000	0	0.5718	0.00481
44	0	7000000	0	0	4500000	0	4000000	2500000	1500000	1000000	0.6640	0.00248
45	4000000	3500000	500000	3500000	3000000	1500000	2500000	0	2000000	0	0.4363	0.00309

Table 2
Optimal DQN extra-structural damping distribution for near-fault events. Units of measure is [N·sec/m].

Earthq. #	*Level 1*	*Level 2*	*Level 3*	*Level 4*	*Level 5*	*Level 6*	*Level 7*	*Level 8*	*Level 9*	*Level 10*	*Gini index*	*Peak interstory drift [m]*
46	0	3500000	1000000	4000000	4500000	0	2000000	2500000	2000000	1000000	0.4634	0.00673
47	5500000	3500000	3000000	4000000	1000000	3000000	0	0	500000	0	0.5664	0.01870
48	6500000	3500000	0	4500000	4500000	0	0	0	1500000	0	0.6748	0.01495
49	0	6000000	0	4000000	3500000	3500000	3500000	0	0	0	0.6152	0.02032
50	0	4500000	0	1500000	6000000	4500000	1500000	500000	0	2000000	0.6098	0.01496
51	1500000	7500000	0	3500000	0	0	2000000	3500000	2500000	0	0.6369	0.02128
52	2000000	4000000	0	3500000	3500000	0	1500000	4000000	500000	1500000	0.4634	0.01145
53	0	8000000	0	1500000	0	0	3000000	4000000	2500000	1500000	0.6640	0.01144
54	500000	5500000	0	2000000	500000	1000000	2000000	3500000	3500000	2000000	0.4797	0.02301
55	1000000	0	0	1500000	2000000	4000000	3000000	4500000	3000000	1500000	0.4526	0.00613
56	0	5500000	0	4500000	2000000	0	1000000	3000000	2500000	2000000	0.5447	0.02609
57	6500000	0	1500000	3000000	0	3500000	2500000	2000000	0	1500000	0.5501	0.01801
58	0	6000000	0	4500000	3500000	4000000	0	0	2500000	0	0.6423	0.01622
59	9000000	0	0	7000000	0	3000000	0	0	0	1500000	0.8103	0.04372
60	6000000	2000000	0	3500000	0	3500000	2000000	2000000	0	1500000	0.5285	0.01817
61	2500000	0	0	7000000	0	4000000	0	3500000	2000000	1500000	0.6314	0.04266
62	5500000	4500000	0	5000000	0	3000000	500000	2000000	0	0	0.6369	0.02695
63	6500000	0	0	0	1500000	3500000	3500000	2500000	1500000	1500000	0.5610	0.05682
64	5500000	500000	0	4500000	4000000	2000000	0	2500000	0	1500000	0.5827	0.03818
65	0	5500000	0	500000	500000	5000000	5000000	0	2500000	1500000	0.6314	0.02095
66	6500000	0	0	3500000	0	3500000	0	3500000	2000000	1500000	0.6043	0.03199
67	0	5000000	0	1000000	1000000	5000000	4500000	0	2500000	1500000	0.5827	0.05615
68	5500000	4000000	0	3500000	0	1000000	2500000	2000000	2000000	0	0.5393	0.02757
69	2500000	3000000	4500000	1000000	500000	0	2000000	3000000	2500000	1500000	0.3875	0.00701
70	0	5000000	0	4500000	0	1500000	3000000	2500000	2500000	1500000	0.5176	0.02753
71	3000000	2500000	0	3500000	3500000	1500000	2000000	2000000	1500000	1000000	0.3225	0.01515
72	0	0	0	7000000	0	4500000	3000000	2500000	2000000	1500000	0.6369	0.01051
73	0	0	0	7000000	5500000	5500000	0	2500000	0	0	0.7398	0.03195
74	7500000	0	0	3500000	2000000	3000000	0	3000000	0	1500000	0.6314	0.00890
75	0	5000000	0	4500000	4000000	0	3000000	2500000	0	1500000	0.5772	0.00890
76	6500000	0	0	4000000	0	5500000	4500000	0	0	0	0.7127	0.02585
77	0	4000000	4000000	2500000	3500000	3000000	0	2000000	0	1500000	0.4688	0.01202
78	4500000	2000000	0	5000000	500000	1500000	2500000	2500000	2000000	0	0.4851	0.01409
79	5500000	4000000	0	0	4500000	0	3000000	1500000	2000000	0	0.5989	0.01075
80	5500000	0	0	3500000	0	5500000	0	2000000	2500000	1500000	0.6152	0.00453
81	3000000	3500000	0	1500000	3500000	4500000	0	4000000	500000	0	0.5230	0.00934
82	6500000	0	0	0	2000000	5500000	0	2500000	2500000	1500000	0.6369	0.01627
83	6000000	0	0	4500000	0	3000000	3000000	2000000	1000000	1000000	0.5827	0.00953
84	5500000	3000000	0	3000000	2000000	3500000	0	2500000	0	1000000	0.5176	0.00646
85	0	5500000	0	5000000	0	3000000	3000000	0	2500000	1500000	0.5935	0.01055

incoming seismic excitation. This graph highlights the concentration index ranging from 0.4 to 0.8, corresponding to a medium-high value. The only values outside this range are observed for some near-fault events, which correspond to both the maximum and minimum concentration of the extra-structural viscous dampers in the levels.

In Fig. 16, for every seismic record, the maximum value of the peak interstory displacements, Eq. (11), corresponding to the optimal distribution of the devices is shown. The greater seismic demand associated with near-fault events is evident. In some cases, even the optimal allocation of viscous dampers does not make it possible to limit the peak interstory displacement to below 3 cm. Figs. 17 and 18 represent data that are not included in Table 1-Table 2. Fig. 17 represents the level at which the maximum value of the peak interstory displacements is related. This representation shows that, in most cases, the maximum value of the peak displacements occurs at the first level, more rarely, at the middle floors (i.e., the fifth and sixth levels). Rarer are the occurrences at the other floors.

Fig. 18 plots the non-dimensional ratio of Eq. (13):

$$\zeta = \frac{\max(x_i^{peak}) - \min(x_i^{peak})}{\min(x_i^{peak})} \quad i = 1, 2, 3..., 10 \tag{13}$$

which represents an absolute performance index of the optimal placement strategy for the different ground motions. This index measures the uniformity among the interstory displacements obtained through the optimal arrangement of extra-structural devices. In fact, this index should be reduced as much as possible to make the seismic demand uniformly distributed in the levels of the structure. However, this possibility is constrained by the number of devices used to achieve a certain level of damping, as well as by the dynamic characteristics of the input excitation. The results reveal that near-fault ground motions tend to require a greater allocation of viscous dampers at the lower stories compared to far-field events. This pattern can be attributed to the particular features of near-fault seismic excitations, which are often characterized by intense, long-period velocity pulses that induce substantial base shear and large interstory drifts concentrated at the lower levels of the structure. Previous studies [88,89] have demonstrated that such impulsive inputs produce a significant concentration of deformation demands at the base, thereby justifying the strategic placement of energy dissipation devices at these stories to enhance overall seismic performance. Conversely, far-field ground motions, typically exhibiting a wider frequency content and lacking strong velocity pulses, tend to generate a more distributed seismic demand along the height, even though the dominance of the first vibration mode still leads to a preferential, albeit less pronounced, concentration of dampers toward the lower part of the structure. Moreover, the results clearly highlight the importance of the characteristics of the incoming seismic excitation in relation to the optimal placement of the devices. Even in the case of seismic excitations described by very similar values of the synthetic indices, significantly different optimal distributions of the viscous dampers along the height of the structure are obtained. This means that it does not exist a reliable regression analysis able to relate the synthetic parameters of the optimal distribution and the considered seismic parameters. Moreover, this underlines the need for advanced tools, such as the one herein proposed, to evaluate not only the optimal solution but, more importantly, its robustness with respect to the randomness of

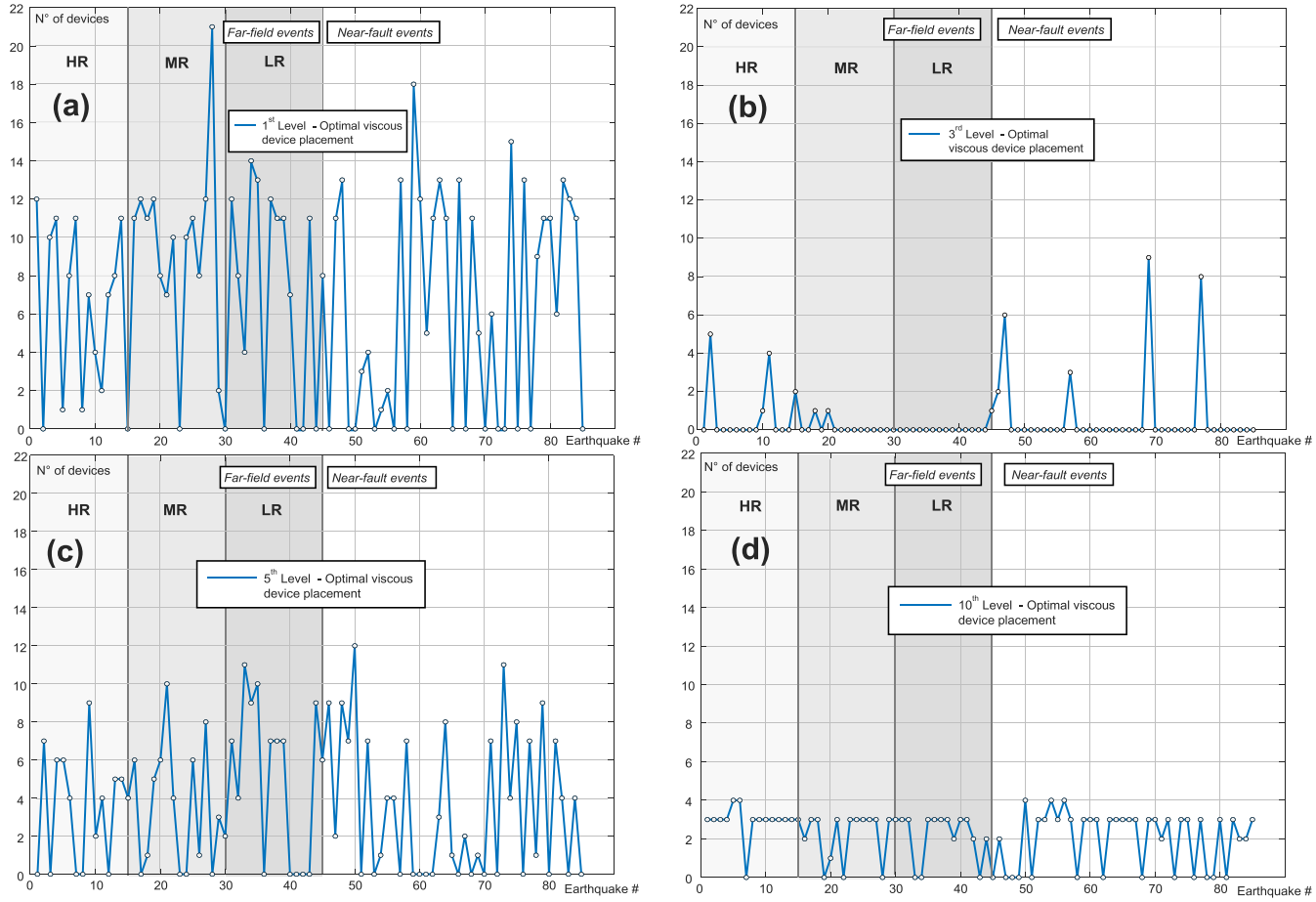

Fig. 14. Number of devices optimally located at the different levels.

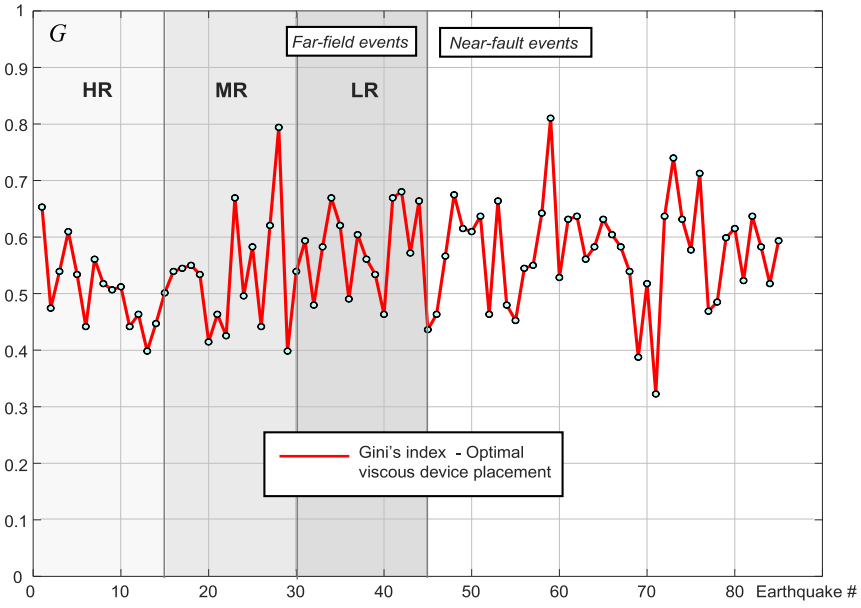

Fig. 15. Gini concentration index for the optimal placement of devices.

seismic excitations.

6. Effectiveness of the proposed DQN algorithm

As emphasized in Section 4, each seismic excitation represents a different environment for the DQN agent. One of the objectives of this

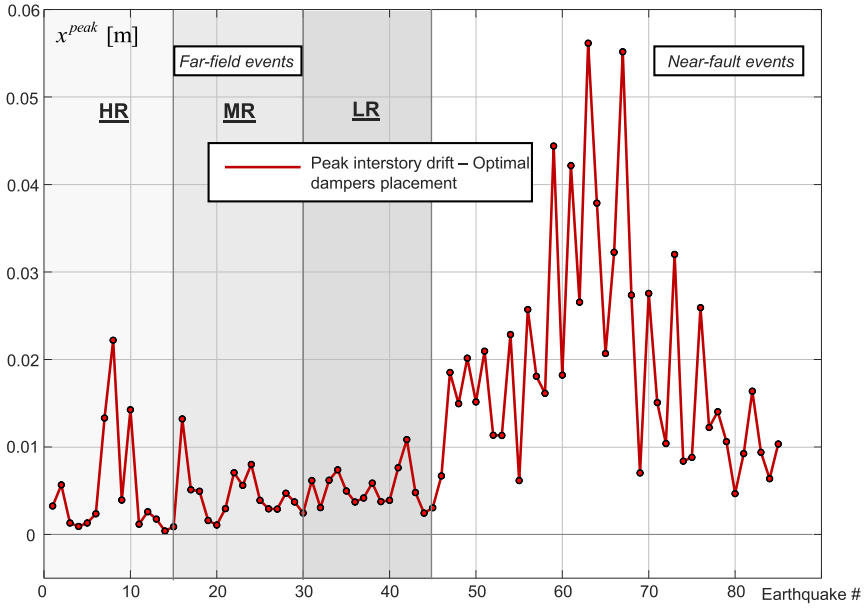

Fig. 16. Maximum value of the peak interstory drifts across levels for the optimal placement of devices.

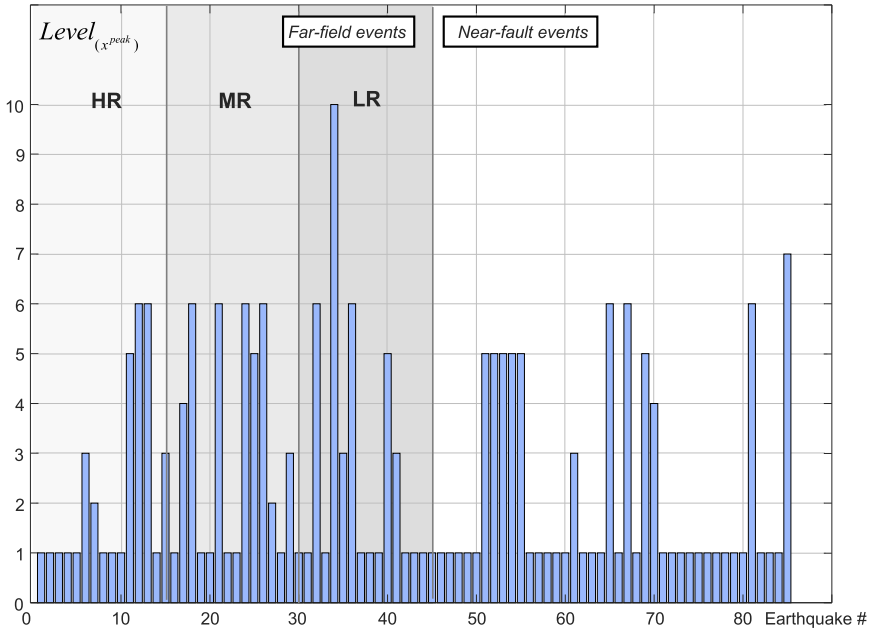

Fig. 17. Level of the maximum value of the peak interstory drifts for the optimal placement of devices.

work is to demonstrate that the effectiveness of the proposed algorithm is high despite variations in the characteristics of the incoming ground motions. With this aim, three specific analyses were carried out and described in the following subsections to test the performance achievable through the obtained optimal distributions of the viscous dampers.

6.1. DQN algorithm vs uniform damping distribution

The considered benchmark structure exhibits a first mode characterized by a perfectly uniform deformed shape along the height, with equal inter-story modal components at all floors (Fig. 3). A key consequence of this structural regularity is that engineering heuristics commonly proposed as baseline strategies for damper placement, such as distributions proportional to mode shape amplitude, story shear, or drift profile of the undamped structure, all converge exactly to the uniform distribution for this structural system. The uniform distribution therefore already represents the most informed engineering heuristic applicable to this structure. In this situation, the existing literature [90–92] suggests that such a uniform distribution of damping may represent a suboptimal solution to the addressed problem. It thus follows a comparison between the seismic demand in terms of interstory displacements obtained through the identified optimal solution and the one derivable from a uniform distribution of damping across the different levels: $c_i = 2050000\text{Nsec/m}$ for $i = 1,2,3...,10$. Fig. 19 and Fig. 20 show the time histories in terms of interstory displacement for each structural level within the two considered distributions, optimal (i.e., DQN algorithm) (a) and uniform (b), respectively, in the case of a far-field excitation, earthquake #24, and a near-fault one, earthquake #77. These figures emphasize the substantial difference in the system's response: in the first case (Fig. 19), the uniform solution can be considered

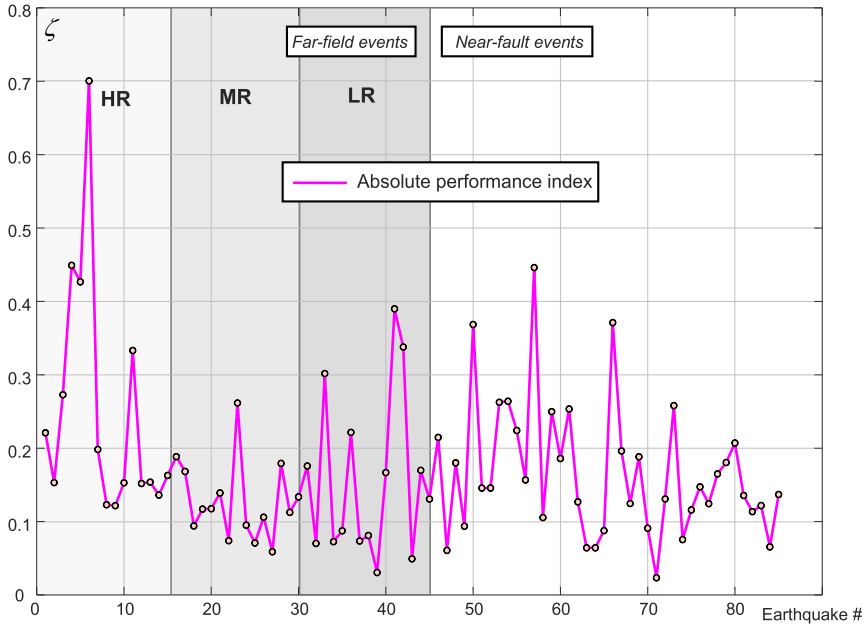

Fig. 18. Absolute performance index for the optimal placement of devices.

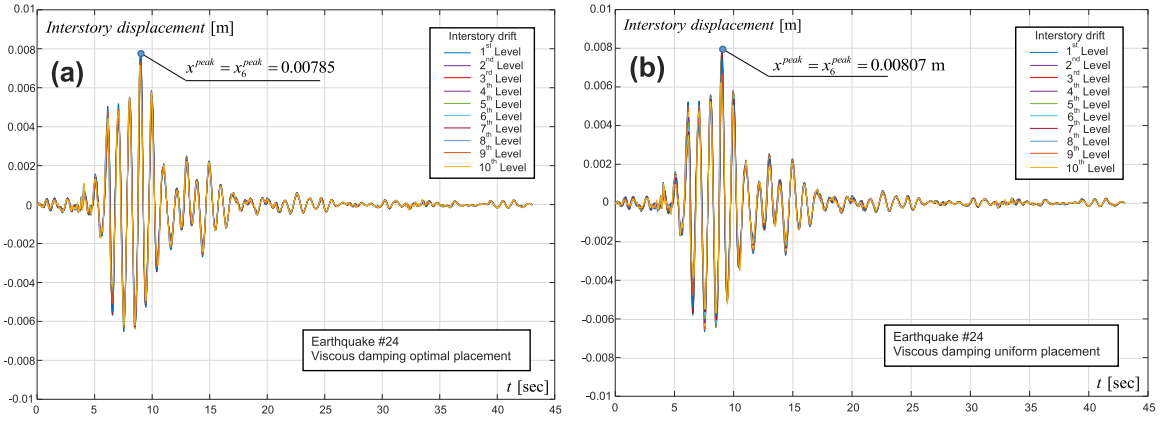

Fig. 19. Interstory displacement time-history for earthquake #24 – optimal vs uniform distribution.

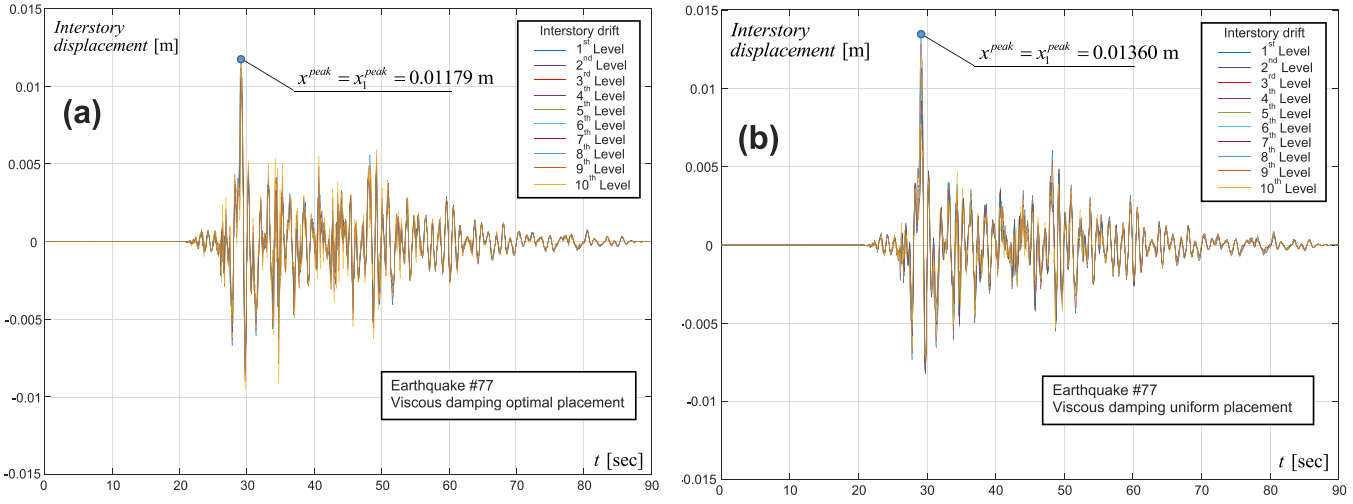

Fig. 20. Interstory displacement time-history for earthquake #77 – optimal vs uniform distribution.

equivalent to the optimal one in terms of seismic performance, while in the second case (Fig. 20), the difference is significant and can dramatically increase the level of damage. By considering all the seismic events, Fig. 21 shows the comparison between the two alternative damping distributions in terms of a dimensionless factor, Eq. (14), that is the percentage reduction achieved between the uniform distribution to the optimal one according to the proposed DQN algorithm:

$$\Delta\rho_{\%} = \frac{\max(x_{i,unif}^{peak}) - \max(x_{i,DQN}^{peak})}{\max(x_{i,unif}^{peak})} \quad i = 1, 2, 3..., 10 \tag{14}$$

The results show that the optimal distribution allows, in all cases, to achieve a reduction in the maximum value of the peak interstory displacements. This reduction is highly variable, ranging from a minimum of 1%, where the uniform distribution can be considered a suboptimal solution, to maximum values of 13%. Consequently, the comparison illustrates that the damper configuration achieved through the DQN method demonstrates superior performance compared to the uniform distribution, which is typically recommended by seismic codes for regular structures, such as the structure examined. In many cases, the results are significantly improved, highlighting the potential for a substantial reduction in structural damage.

6.2. Verification of the local minimum points of the obtained solution

A sensitivity analysis regarding the optimal placement of devices is carried out by evaluating the maximum value of the peak interstory drifts across all stories in all possible configurations of the devices obtained by shifting a single device from one floor to another, starting from the optimal configuration. The results of this analysis are depicted in Fig. 22 for earthquake #1, where a sensitivity matrix, with the original levels on the rows and the destination levels on the columns, shows the variation in maximum value of the peak interstory displacements deriving from this analysis. From Fig. 22, it is deducible that the solution identified by the DQN algorithm indeed corresponds to a minimum point of the objective function for earthquake #1, as any possible action leads to a positive variation, i.e., an increase in seismic demand in terms of maximum value of the peak interstory displacements.

This type of analysis was carried out for all the seismic signals considered. In 83 out of 85 cases, the situation is similar to the case presented, with the DQN algorithm being able to identify the local minimum. In only 2 cases, referring to near-fault earthquakes, the solution found was not optimal; in particular, the two sensitivity matrices present a single negative value, suggesting that the performance obtained can be improved by moving a device between two floors.

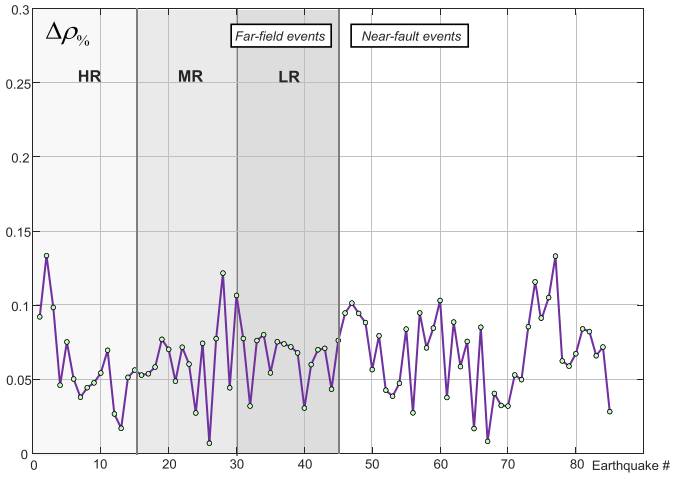

Fig. 21. Non-dimensional reduction factor moving from uniform to optimal devices distribution.

Regarding these two cases in which the DQN algorithm failed to capture the optimal solution, the explanation is related to the unique characteristics of near-fault earthquakes, which often produce high-amplitude pulses and consequently more complex dynamic responses. Such pulses can lead to rapid shifts in structural demands, making it challenging for the RL algorithm to balance exploration and exploitation within the number of episodes considered.

6.3. Comparison of DQN algorithm with gradient descent, genetic algorithm and particle swarm optimization

The first optimization technique compared with the DQN algorithm is the gradient descent method (GD), for its features in terms of convergence behaviour, computational cost and ease of implementation [93,94]. This approach minimizes a cost function $\rho = J(\boldsymbol{\theta})$ where $\boldsymbol{\theta}$ is a vector of parameters by iteratively moving in the direction of the steepest descent. The step size, or learning rate, defines the magnitude of each update, and iterations continue until no further reduction in the function value is achieved, indicating convergence to a local minimum. In this study, the cost function corresponds to the maximum value of the peak interstory drifts across all levels, while the parameter vector, size 10, represents the additional damping values for each level, as expressed in:

$$\rho = J(\boldsymbol{\theta}) = J(c_1, c_2, c_3, c_4, c_5, c_6, c_7, c_8, c_9, c_{10}) \text{with} \sum_{i=1}^{10} c_i = C_{tot} \tag{15}$$

and the gradient was computed through a discrete sensitivity analysis, in which the cost function variation was evaluated by perturbing one damping device at a time. In this context, the learning rate is defined as the allocation of a single device, representing the elementary step of the optimization process. Given the problem's strong non-linearity and non-convexity, the results depend on the initial point. To mitigate entrapment in local minima, random initialization was adopted [95]: for each seismic excitation, 2000 random structural configurations were generated and optimized using gradient descent.

The second optimization method compared with the DQN algorithm is the Genetic Algorithm (GA), a stochastic, population-based metaheuristic inspired by natural selection principles [96,97]. The algorithm searches for the optimal configuration of damping devices by evolving a population of candidate solution $\boldsymbol{\theta} = [c_1, \ldots, c_{10}]$ through selection, crossover and mutation operators. The objective function to be minimized corresponds to that given in Eq. (15). In detail, the GA used a population of 200 individuals evolved over a maximum of 300 generations, with a crossover fraction of 0.8 and uniform mutation.

The third optimization technique considered is Particle Swarm Optimization (PSO), which also belongs to the class of metaheuristic algorithms and is inspired by the social behavior of swarms [98,99]. Each particle represents a candidate configuration of the damping devices, $\boldsymbol{\theta}$, and is associated with a velocity vector that guides its movement in the search space. The fitness of each particle is evaluated using the cost function defined in Eq. (15). At each iteration, a particle updates its position based on three components: its previous velocity scaled by the inertia weight ω, the cognitive coefficient ϕ_p and the social coefficient ϕ_g [98,99]. In the present analysis, the swarm consisted of 100 particles evolving over 50 iterations, with inertia weight $\omega = 0.7$ and cognitive/social coefficients $\phi_p = \phi_g = 1.5$. For indicative reference, on a standard personal computer the DQN algorithm required approximately 10–15 min per seismic record, compared to 5–8 min for GD, 5–10 min for GA, and 15–25 min for PSO. These time intervals are consistent with the requirements of a standard engineering design process, where the framework is intended to be applied to a limited set of site-specific records rather than in a real-time context.

The results concerning effectiveness comparison between the different minimization algorithms are presented in Fig. 23-Fig. 24. Specifically, Fig. 23 represent, for each seismic excitation, the following

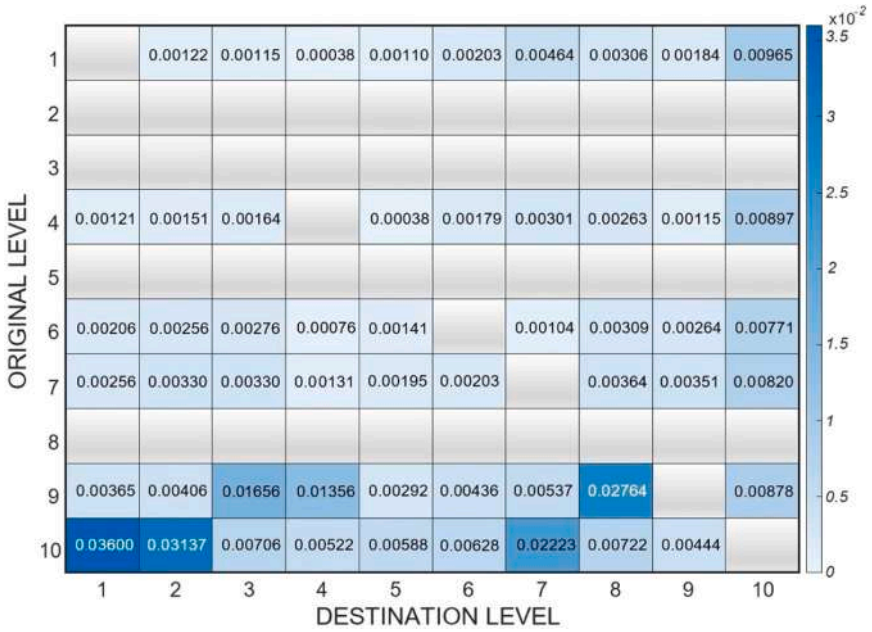

Fig. 22. Variation in maximum value of the peak interstory drifts [cm] due to the relocation of a single damping device for earthquake #1.

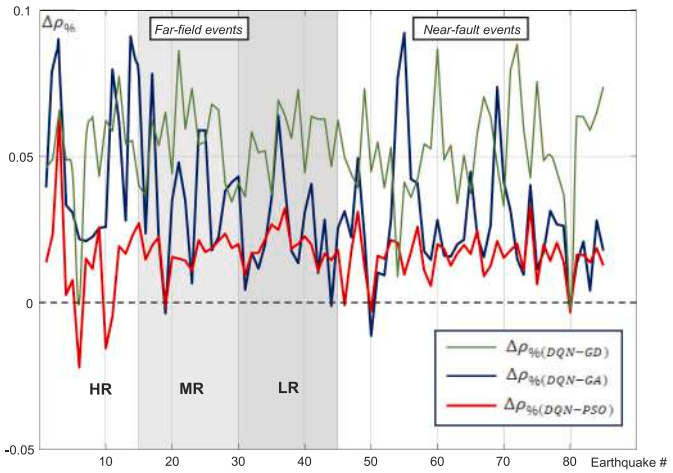

Fig. 23. Comparison between the performances achievable by the different optimization algorithms considered.

performance indexes:

$$\Delta\rho_{\%(DQN-GD)} = \frac{\max(x_{i,GD}^{peak}) - \max(x_{i,DQN}^{peak})}{\max(x_{i,GD}^{peak})} \quad i = 1, 2, 3..., 10 \tag{16}$$

$$\Delta\rho_{\%((DQN-GA)} = \frac{\max(x_{i,GA}^{peak}) - \max(x_{i,DQN}^{peak})}{\max(x_{i,GA}^{peak})} \quad i = 1, 2, 3..., 10 \tag{17}$$

$$\Delta\rho_{\%((DQN-PSO)} = \frac{\max(x_{i,PSO}^{peak}) - \max(x_{i,DQN}^{peak})}{\max(x_{i,PSO}^{peak})} \quad i = 1, 2, 3..., 10 \tag{18}$$

defined analogously to Eq. (14) and representing the gain in terms of maximum value of the peak interstory displacements obtained with the DQN compared to the other three strategies. This leads to define three curves where an index value below 0 indicates that the DQN performs worse than the corresponding method. The obtained results demonstrate the effectiveness of the DQN-based approach in addressing the considered optimization problem.

In general, the three alternative optimization methods yield higher interstory drift values for the majority of the seismic excitations analyzed. Notable exceptions are observed for certain excitations within the far-field HR group, where the PSO algorithm exhibits superior performance, and for two far-field excitations (i.e., earthquakes #50 and #80), where the DQN algorithm shows reduced efficiency, providing less favorable results compared to the other techniques considered. The two excitations for which the DQN shows reduced efficiency correspond precisely to the near-fault records identified in Section 6.2 as cases where the algorithm did not converge to a local minimum of the objective function. However, the improvement achieved by the alternative methods for these two records remains limited to less than 1% in terms of peak interstory drift, confirming that the complexity of the objective function landscape associated with these particular near-fault excitations represents a challenge for all optimization methods considered, rather than a specific limitation of the proposed approach. In addition, to summarize the superiority of the DQN-based design algorithm, the mean percentage reduction in maximum value of the peak interstory displacements achieved by the DQN approach, with respect to the three alternative algorithms as well as to the uniform damping distribution, was computed over the 85 seismic excitations. These results are reported in Table 3, where a negative minimum improvement indicates that there exists at least one case in which the DQN algorithm yields higher interstory drift values. On average, only the PSO algorithm exhibits performance values close to those achieved by the proposed approach. Furthermore, the comparative analysis confirms that the characteristics of the input seismic excitation significantly influence the variability among the optimal solutions obtained by the different algorithms.

Regarding the computation times, all numerical developments were carried out with the same equipment and in Matlab. The proposed approach was slightly more demanding than the GD and GA algorithms, whereas the PSO algorithm was strongly more computationally intensive. As expected, these times are influenced by the specific choices of metaparameters adopted for each algorithm. The selected configurations were defined based on the existing literature on similar problems [93]– [99] and through an appropriate compromise between the available computational capacity and the stability of the obtained results.

For the sake of comprehensiveness, the optimal retrofitting

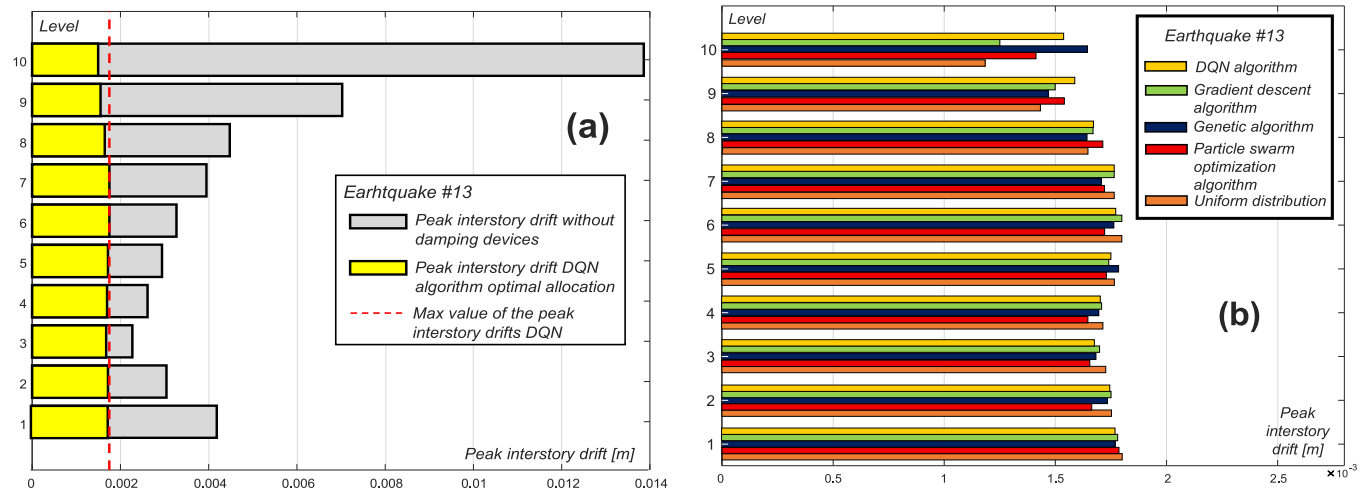

Fig. 24. Peak interstory drift demand – Benchmark structure, earthquake #13.

Table 3
Comparison of Drift Reductions between DQN, Uniform Distribution and Gradient Descent Algorithm.

Comparison	Average Drift Reduction over the 85 seismic events (%)	Maximum improvement over the 85 seismic events (%)	Minimum improvement over the 85 seismic events (%)
DQN vs uniform distribution	6.43	13.10	1.22
DQN vs gradient descent algorithm	5.39	8.89	−0.39
DQN vs genetic algorithm	4.56	9.32	−1.16
DQN vs particle swarm optimization	1.63	6.11	−2.32

configurations are also compared to the configuration without viscous dampers. Specifically, the no-retrofitted benchmark structure exhibits the maximum value of the peak interstory displacements at the 10th story for the majority of the seismic records considered (Fig. 7(b)), with the distribution of the seismic demand varying across the stories depending on the specific ground motion (Fig. 7(c)). The inclusion of viscous dampers leads to a substantial redistribution of the seismic demand. Fig. 24 illustrates the peak interstory drift for a representative earthquake (i.e., earthquake #13), comparing the case without dampers (Fig. 24(a)) with those obtained using uniform, gradient descent-based, genetic algorithm, particle swarm optimization and DQN-based damping distributions (Fig. 24(b)). The results, which can be extended, as observed, to most of the seismic excitations considered, clearly demonstrate that the inclusion of viscous dampers reduces and homogenizes the seismic demand across the various stories of the structure. The DQN algorithm outperforms the alternative approaches in terms of maximum value of the peak interstory drifts (Fig. 24(b)).

7. Conclusions

7.1. Summary of findings

The main findings of the present study can be summarized as follows:

- A DQN-based framework for the optimal placement of viscous dampers in multi-story elastic frames has been successfully formulated and implemented, demonstrating that the problem can be effectively cast as a discrete reinforcement learning task with acceptable computational costs;
- For all 85 seismic records considered, the DQN approach yields improved performance compared to the uniform damping distribution, which represents the most informed engineering heuristic for the regular benchmark structure adopted;
- Near-fault excitations generally lead to higher interstory drift demands and more concentrated damper distributions, reflected by consistently high Gini index values, with devices preferentially placed at lower stories due to the impulsive nature of near-fault ground motions. Far-field scenarios instead produce more distributed damping solutions with lower overall drift demands;
- The sensitivity analysis confirmed that 83 out of 85 identified solutions correspond to local minimum points of the objective function. In the remaining 2 near-fault cases, the suboptimality is marginal and the improvement achievable by alternative methods remains below 1%;
- The proposed algorithm compares favorably with Gradient Descent, Genetic Algorithm and Particle Swarm Optimization in terms of solution quality, confirming its effectiveness across a wide range of seismic input characteristics;
- The results highlight that the optimal damper placement is strongly dependent on the characteristics of the incoming seismic excitation, an aspect largely overlooked in the existing literature, underscoring the need for advanced optimization tools such as the one proposed;
- Based on the overall evidence, the proposed design algorithm can certainly be considered a promising approach in terms of efficiency and robustness with respect to the characteristics of the incoming seismic excitations, even considering the strong non-linearity that characterizes the environment in which the agent operates.

7.2. Future research directions

The proposed framework is conceptually extensible to more complex structural configurations, including cases involving concentrated or distributed nonlinearities and irregular structures with global and local failure mechanisms, although such extensions would require substantially higher computational resources. Further planned developments concern the study of eventual non-linear response of structures together with the definition of a more comprehensive reward function incorporating the installation costs of the damping devices at different floors, as well as the direct and indirect costs associated with seismic damage, providing a more complete basis for performance-based seismic design. Finally, how to aggregate the optimal configurations obtained for multiple site-specific records into a single design solution, represents

another future research direction.

Declaration of Competing Interest

The authors declare that they have no known competing financial interests or personal relationships that could have appeared to influence the work reported in this paper.

Acknowledgments

This study was carried out within the «Data fusion based digital twins for structural safety assessment» project – funded by European Union – Next Generation EU within the PRIN 2022 program (D.D. 104 - 02/02/2022 Ministero dell'Università e della Ricerca). This manuscript reflects only the authors' views and opinions and the Ministry cannot be considered responsible for them. This study was also carried out within the RETURN Extended Partnership and received funding from the European Union Next-GenerationEU (National Recovery and Resilience Plan—NRRP, Mission 4, Component 2, Investment 1.3—D.D. 1243 2/8/2022, PE0000005). This work is also part of the research activity developed by the authors within the framework of the "PNRR": MOST–Sustainable Mobility National Research Center - SPOKE 7 "Cooperative Connected and Automated Mobility and Smart Infrastructures" - WP4" and received funding from the European Union Next-GenerationEU (PIANO NAZIONALE DI RIPRESA E RESILIENZA (PNRR) – MISSIONE 4 COMPONENTE 2, INVESTIMENTO 1.4 – D.D. 1033 17/06/2022).

Data Availability

Some or all data, models or code that support the findings of this study are available from the corresponding author upon reasonable request.

References

[1] Kelly JM. Aseismic base isolation: review and bibliography. Soil Dyn Earthq Eng 1986;5(4):202–16.
[2] Megget LM. Analysis and design of a base-isolated reinforced concrete frame building. Bull NZ Soc Earthq Eng 1978;11(4):245–54.
[3] Pall AS, Marsh C. Response of friction damped braced frames. J Struct Div 1982;108(6):1313–23.
[4] Makris N, Constantinou MC. Fractional-derivative Maxwell model for viscous dampers. J Struct Eng ASCE 1991;117(9):2708–24.
[5] Makris N, Constantinou MC. Spring-viscous damper systems for combined seismic and vibration isolation. Earthq Eng & Struct Dyn 1992;21(8):649–64.
[6] Constantinou MC, Symans MD, Tsopelas P, Taylor DP. Fluid Viscous Dampers in Applications of Seismic Energy Dissipation and Seismic Isolation, ATC-17-1 Seminar on Seismic Isolation, Passive Energy Dissipation, and Active Control, San Francisco. CA 1993;1993:581–92.
[7] Tyler RG. Tapered steel energy dissipators for earthquake resistant structures. Bull NZ Soc Earthq Eng 1978;11(4):282–94.
[8] De Iuliis M, Petti L, Palazzo B. Combined control strategy base isolation and tuned mass damper: An effectiveness analysis of its application to non-linear benchmark base isolated structure. Proceedings of the 14th World Conference on Earthquake Engineering, Beijing, China. 2008. 12–17 October.
[9] Alwilly G, Lavan O. Optimal seismic design of multiple isolation systems and viscous dampers in vertically irregular frame buildings. Earthq Eng & Struct Dyn 2025;0:1–19.
[10] American Society of Civil Engineers. Minimum design loads and associated criteria for buildings and other structures (ASCE-SEI 7-22). American Society of Civil Engineers; 2022.
[11] Japan Building Code. Seismic design specifications. Minist Land Infrastruct Transp Tour 2021.
[12] MIT. NTC 2018: D.M. del Ministero delle Infrastrutture e dei trasporti del 17/01/2018. Aggiornamento delle Norme Tec per Le Costr (Ital) 2018.
[13] Takewaki I. Optimal damper placement for minimum transfer functions. Earthq Eng & Struct Dyn 1997;26(11):1113–24.
[14] Lopez-Garcia D. A simple method for the design of optimal damper configurations in MDOF structures. Earthq Spectra 2001;17(3):387–98.
[15] Aydin E, Boduroglu MH, Guney D. Optimal damper distribution for seismic rehabilitation of planar building structures. Eng Struct 2007;29(2):176–85.
[16] Fujita K, Yamamoto K, Takewaki I. An evolutionary algorithm for optimal damper placement to minimize interstorey-drift transfer function in shear building. Earth Str 2010;1(3):289–306.
[17] Lavan O, Levy R. Optimal design of supplemental viscous dampers for linear framed structures. Earthq Eng & Struct Dyn 2006;35(3):337–56.
[18] Lavan O, Dargush GF. Multi-objective evolutionary seismic design with passive energy dissipation systems. J Earthq Eng 2009;13(6):758–90.
[19] Adachi F, Yoshitomi S, Tsuji M, Takewaki I. Nonlinear optimal oil damper design in seismically controlled multi-story building frame. Soil Dyn Earthq Eng 2013;44:1–13.
[20] Yahyazadeh A, Yakhchalian M. Probabilistic residual drift assessment of SMRFs with linear and nonlinear viscous dampers. J Constr Steel Res 2018;148:409–21.
[21] Patil MB, Ramakrishna U, Mohan SC. Multi-objective optimisation of damper placement for improved seismic response in dynamically similar adjacent buildings. Sādhanā 2020;45:1–12.
[22] R.E. Perez RE, Behdinan K. Particle swarm approach for structural design optimization. Comput & Struct 2007;85(19–20):1579–88.
[23] Movaffaghi H, Friberg O. Optimal placement of dampers in structures using genetic algorithm. Eng Comput Intern J Comput-Aided Eng 2006;23:597–606.
[24] Gad A. Particle swarm optimization algorithm and its applications: A systematic review. Arch Comput Methods Eng 2022;29:2531–61.
[25] Wongprasert N, Symans M. Application of a Genetic Algorithm for Optimal Damper Distribution within the Nonlinear Seismic Benchmark Building. ASCE J Eng Mech 2004;130(4):401.
[26] Noureldin M, Ali A, Memon S, Kim J. Fragility-based framework for optimal damper placement in low-rise moment-frame buildings using machine learning and genetic algorithm. J Build Eng 2022;54:104641.
[27] Kangda MZ, Bakre S. Performance of linear and nonlinear damper connected buildings under blast and seismic excitations. Innov Infrastruct Solut 2021;6(2):130.
[28] Sanghai S, Pawade P. Optimal placement of friction dampers in building considering nonlinearity of soil. Innov Infrastruct Solut 2021;6:1–18.
[29] Gomez F, Spencer Jr BF, Carrion J. Simultaneous optimization of topology and supplemental damping distribution for buildings subjected to stochastic excitation. Struct Control Health Monit 2021;28(7):e2737.
[30] Akehashi H, Takewaki I. Inverse optimal damper placement via shear model for elastic–plastic moment-resisting frames under large-amplitude ground motions. Eng Struct 2022;250:113457.
[31] Chan PT, Leu LJ, Ma QTM. Optimizing viscous damper placement with element exchange method and energy-based distribution methods for building structures. Int J Struct Stab Dyn 2022;22(15):2250166.
[32] Li L, Liang Y, Chen G, Yang D. Simultaneous layout and size optimization of nonlinear viscous dampers for frame buildings under stochastic seismic excitation. Eng Struct 2022;273:115067.
[33] Hosoda M, Fujita K. Robust optimal damper placement based on robustness index simultaneously considering variation of elastoplastic design criteria and input level. Front Built Environ 2024;10:1353827.
[34] Castaldo P, De Iuliis M. Optimal integrated seismic design of structural and viscoelastic bracing-damper systems. Earthq Eng & Struct Dyn 2014;43(12):1809–27.
[35] Yang J, Liu Y, Niu B, Peng C, Wang T, Xie J, Pan T. Multi-level structural damage identification based on time domain response reconstruction and deep reinforcement learning. Structures 2025;80:107666.
[36] Lin CH, Fu B, Zhang L, Li N, Tong GS. Intelligent design of steel–concrete composite beams based on deep reinforcement learning. Structures 2024;70:107666.
[37] Kim HS, Kim U. Development of a control algorithm for a semi-active mid-story isolation system using reinforcement learning. Appl Sci 2023;13(4):2053.
[38] Pisarski D. & Jankowski, Ł. Reinf Learn-Based Control suppress transient Vib semi-Act Struct Subj Unkn Harmon Excit Comput-Aided Civil Infrastruct Eng 2023;38(12):1605–21.
[39] Jedlińska A, Pisarski D, Mikułowski G, Błachowski B, Jankowski Ł. Semi-active structural control using viscous dampers and reinforcement learning. X ECCOMAS Themat Conf SMART Struct Mater (SMART 2023) 2023, July.
[40] Panda J, Chopra M, Matsagar V, Chakraborty S. An iterative gradient descent-based reinforcement learning policy for active control of structural vibrations. Com & Struct 2024;290:107183.
[41] Gheni EZ, Al-Khafaji HM, Alwan HM. A deep reinforcement learning framework to modify LQR for an active vibration control applied to 2D building models. Open Eng 2024;14(1):20220496.
[42] Cao L, Pan H, Li X, Li C. Predicting optimal primary tuning parameters of PTTMDI for vortex-induced vibration control of super-tall buildings using physics information enhanced DNN. Eng Struct 2025;334:120268.
[43] Li C, Zhao J, Pan H, Cao L, Guan Q, Xu Z-D. Deep reinforcement learning based performance optimization of hybrid system for base-isolated structure and shape memory alloy-inerter. Eng Struct 2025;334:120244.
[44] Li X, Wang Z, Pan H, Cao L, Li C. Hybrid system of base-isolated structures with tuned mass damper-inerters considering internal friction. J Build Eng 2025;101:11853.
[45] Li X, Zhou C, Shu W, Li C, Cao L. Soil-damped structure interaction analysis considering deep reinforcement learning-driven soil mesh optimization. Soil Dyn Earthq Eng 2026;202:110067.
[46] Kookalani S, Shen D, Zhu LL, Lindsey M. An overview of optimal damper placement methods in structures. Iran J Sci Technol Trans Civil Eng 2022:1–20.
[47] CEN – European Committee for Standardization. Eurocode 8: Design of structures for earthquake resistance – Part 1: General rules, seismic actions and rules for buildings (EN 1998-1:2004). Brussels, Belgium: European Committee for Standardization; 2004.
[48] Nemirovski A, Yudin D. Problem Complexity and Method Efficiency in Optimization. New York: Wiley; 1983.

[49] Reeves CR, Rowe JE. Genetic Algorithms: Principles and Perspectives. A guide to GA Theory. Operations Research/Computer Science Interfaces Series. New York: Springer; 2002.
[50] Kennedy, J., Eberhart, R. (1995) Particle Swarm Optimization. Proceedings of IEEE International Conference on Neural Networks IV., pp. 1942-1948.
[51] Constantinou MC, Symans MD, Taylor DP, Dargush GF. Fluid viscous dampers in applications of seismic energy dissipation and isolation. *ATC-17-1 Seminar on Seismic Isolation, Passive Energy Dissipation and Active Control*, Applied Tech. Cou., San Francisco. CA 1993:581–92.
[52] Dall'Asta A, Tubaldi E, Ragni L. Optimization of nonlinear fluid viscous dampers for building structures: Energy-based design approach under stochastic seismic excitation. Earthq Eng & Struct Dyn 2019;48(12):1451–72.
[53] Del Gobbo GM, Blakeborough A, Williams MS. Improving total-building seismic performance using linear fluid viscous dampers. Bull Earthq Eng 2018;16(9): 4249–72.
[54] EN 15129: CEN – European Committee for Standardization. Anti-seismic devices (EN 15129:2009). Brussels, Belgium: European Committee for Standardization; 2009.
[55] Aiken ID, Kelly JM. Cyclic dynamic testing of fluid viscous dampers. In C. U. Sacramento (Ed.). Proc Caltrans Fourth Seism Res Conf 1996:1–9.
[56] De Iuliis M, Miceli E, Castaldo P. An energy framework to control viscoelastic semi-active devices in plan-wise one-way asymmetric systems. Struct Control Health Monit 2025. 10.1155/stc/7091316.
[57] Pollini N. Fail-safe optimization of viscous dampers for seismic retrofitting. Earthq Eng Struct Dyn 2020;49(15):1599–618.
[58] Levy R, Marianchik E, Rutenberg A, Segal F. A simple approach to the seismic design of friction damped braced medium-rise frames. Eng Struct 2001;23(3): 250–9.
[59] Lavan O, Levy R. Optimal design of supplemental viscous dampers for linear framed structures. Earthq Eng & Struct Dyn 2006;35(3):337–56.
[60] Enidine Inc. (n.d.). Seismic products catalog. Retrieved April 27, 2025, from https://www.enidine.com/getmedia/380757c4-911f-4c67-b97d-1dc6f075acd0/Seismic_Products_Catalog.pdf.
[61] Castaldo P, Miceli E. Optimal single concave sliding device properties for isolated multi-span continuous deck bridges depending on the ground motion characteristics. Soil Dyn Earthq Eng 2023;173:108128.
[62] Zhu TJ, Tso WK, Heidebrecht AC. Effect of peak ground a/v ratio on structural damage. J Struct Eng 1988;114(5):1019–37.
[63] Tso WK, Zhu TJ, Heidebrecht AC. Engineering implication of ground motion A/V ratio. Soil Dyn Earthq Eng 1992;11(3):133–44.
[64] De Iuliis M, Miceli E, Castaldo P. Machine learning modelling of structural response for different seismic signal characteristics: a parametric analysis. Appl Soft Comput 2024;164:112026.
[65] De Iuliis M, Miceli E, Castaldo P. Information theory-guided machine learning to estimate seismic response of non-linear SDOF structures. Eng Struct 2025;336: 120448.
[66] Silver D, Schrittwieser J, Simonyan K, Antonoglou I, Huang A, Guez A, Hassabis D. Mastering the game of go without human knowledge. Nature 2017;550(7676): 354–9.
[67] Levine S, Pastor P, Krizhevsky A, Ibarz J, Quillen D. Learning hand-eye coordination for robotic grasping with deep learning and large-scale data collection. Int J Robot Res 2018;37(4-5):421–36.
[68] Jiang Z, Liang J. Cryptocurrency portfolio management with deep reinforcement learning. 2017 Intelligent systems conference (IntelliSys). IEEE; 2017. p. 905–13.
[69] Peterson EJ, Verstynen TD. A Way Explor-Exploit dilemma bioRxiv 2019:671362.
[70] Sutton RS, Barto AG. Reinforcement learning: An introduction. 2nd ed. The MIT Press; 2018.
[71] Haykin S. Neural networks and learning machines. 3/E. India: Pearson Education; 2009.
[72] Stekolshchik R. Some Approaches Use Overcome overestimation Deep Reinf Learn Algorithms arXiv Prepr arXiv 2020;2006:14167.
[73] Kirkpatrick S, Gelatt Jr CD, Vecchi MP. Optimization by simulated annealing. Science 1983;220(4598):671–80.
[74] Glover F. Future paths for integer programming and links to artificial intelligence. Comput & Oper Res 1986;13(5):533–49.
[75] Crama Y, Kolen AW, Pesch EJ. Local search in combinatorial optimization. Artif Neural Netw Introd ANN Theory Pract 2005:157–74.
[76] Silvestri S, Gasparini G, Trombetti T. A Five-Step Procedure for the Dimensioning of Viscous Dampers to Be Inserted in Building Structures. J Earthq Eng 2010;14(3): 417–47.
[77] Saitua F, Lopez-Garcia D, Taflanidis AA. Optimization of height-wise damper distributions considering practical design issues. Engin Struct 2018;173:768–86.
[78] Federal Emergency Management Agency (FEMA) (2012) Seismic Performance Assessment of Buildings, Volume 1, Methodology. FEMA P-58-1, Washington DC.
[79] Roohi M, Hernandez EM. Performance-based post-earthquake decision making for instrumented buildings. J Civil Struct Health Monit 2020;10:775–92.
[80] Huanga B, Chenb S, Lub W, Mosalam KM. Seismic demand and experimental evaluation of the nonstructural building curtain wall: A review. *Soil Dynamics and Earth*. Engineering 2017;100:16–33.
[81] Kaya YE, Binici B. Data-driven estimation of maximum interstory drift ratio of reinforced concrete frame buildings with deep learning models. J Build Eng 2025; 112:113670.
[82] Mayes RL. Interstory drift design and damage control issues. *The Structural Design of Tall Buildings*. Special Issue. Third Conf Tall Build Seism Reg 1995:15–25.
[83] McFarlane R. A survey of exploration strategies in reinforcement learning. McGill Univ 2018;3:17–8.
[84] Lillicrap TP, Hunt JJ, Pritzel A, Heess N, Erez T, Tassa Y, Silver D, Wierstra D. Continuous control with deep reinforcement learning. Proc 4th Int Conf Learn Represent (ICLR) 2016.
[85] Haarnoja T, Zhou A, Abbeel P, Levine S. Soft actor-critic: Off-policy maximum entropy deep reinforcement learning with a stochastic actor. Proc 35th Int Conf Mach Learn (ICML) 2018;80:1861–70.
[86] Paluszek M, Thomas S, Ham E. Practical MATLAB Deep Learning. A Proj-Based Approach 2022. https://doi.org/10.1007/978-1-4842-7912-0.
[87] Hastie T, Tibshirani R, Friedman J. The Elements of Statistical Learning: Data Mining. Inference, and Prediction. 2nd ed. Springer; 2009.
[88] Alavi B, Krawinkler H. Behavior of moment-resisting frame structures subjected to near-fault ground motions. Earthq Eng & Struct Dyn 2004;33(6):687–706.
[89] Hall JF, Heaton TH, Halling MW, Wald DJ. Near Source Ground Motion and Its Effects on Flexible Buildings. Earthq Spectra 1995;11(4):569–605.
[90] Landi L, Conti F, Diotallevi PP. Effectiveness of different distributions of viscous damping coefficients for the seismic retrofit of regular and irregular RC frames. Eng Struc 2015;100:79–93.
[91] Parajuli S, Pokhrel P, Suwal R. A comprehensive study of viscous damper configurations and vertical damping coefficient distributions for enhanced performance in reinforced concrete structures. Asian J Civil Eng 2024;25(1): 1043–59.
[92] Manchalwar A, Ganpule S, Patil A. Optimal allocation of non-linear viscous dampers for building structures. Asian J Civil Eng 2024:1–13.
[93] Eker E, Kayri M, Ekinci S, İzci D. Comparison of Swarm-based Metaheuristic and Gradient Descent-based Algorithms in Artificial Neural Network Training. ADCAIJ Adv Distrib Comput Artif Intell J 2023;12(1):e29969.
[94] Gómez-Pulido JA, Cortés E, Domínguez A, Lanza-Gutierrez J, Crawford B, Soto R. Comparison Between Stochastic Gradient Descent and VLE Metaheuristic for Optimizing Matrix Factorization. Book Optim Learn 2020:153–64.
[95] Nocedal J, Wright SJ. Numerical Optimization. 2nd Edition. Berlin: Springer-Verlag; 2006.
[96] Movaffaghi H, Friberg O. Optimal placement of dampers in structures using genetic algorithm. Eng Comput 2006;23(6):597–606.
[97] Singh MP, Moreschi LM. Optimal placement of dampers for passive response control. Earthq Eng Struct Dyn 2002;31:955. 76.
[98] Besharatian B, Riahi HT, Garcia R, Hajirasouliha I. Particle swarm optimization of friction tuned mass dampers subjected to ground motion records. *Soil Dynamics and Earth. Eng.* 2023;172:107995.
[99] Guo YQ, Xie WH, Jing X. Study on Structures Incorporated with MR Damping Material Based on PSO Algorithm. Front Mater 2019;6:37.